

Modern Methods of Plant Analysis
New Series Volume 11

Physical

Methods in

Plant Sciences

Edited by
H. F. Linskens and J. F. Jackson



Springer-Verlag

- Coster HGL, Smith JR (1977) Low frequency impedance of *Chara corallina*: simultaneous measurements of separate plasmalemma and tonoplast capacitance and conductance. *Aust J Plant Physiol* 4:667-674
- Ferrier JM (1981) Time-dependent extracellular ion transport. *J Theor Biol* 92:363-368
- Ferrier JM, Dainty J, Ross SM (1985) Theory of negative capacitance in membrane impedance measurements. *J Membrane Biol* 85:245-249
- Graeme JG, Tobey GE, Huelsman LP (1971) Operational amplifier. McGraw Hill, NY
- Homblé F (1985) Effect of sodium, potassium, calcium, magnesium and tetraethylammonium on the transient voltage response to a galvanostatic step and of the temperature on the steady state membrane conductance of *Chara corallina*. *J Exp Bot* 36:1603-1611
- Homblé F (1988) A fast and high-current voltage clamp device for biophysical investigations. *J Phys E: Sci Instrum* 21:1100-1102
- Homblé F, Ferrier JM (1988) Analysis of the diffusion theory of negative capacitance: the role of K^+ and the unstirred layer thickness. *J Theor Biol* 131:183-197
- Homblé F, Jenard A (1984) Pseudo-inductive behaviour of the membrane potential of *Chara corallina* under galvanostatic conditions: a time-variant property of potassium channels. *J Exp Bot* 35:1309-1322
- Homblé F, Jenard A (1986) Membrane operational impedance spectra in *Chara corallina* estimated by Laplace transform analysis. *Plant Physiol* 81:919-921
- Homblé F, Jenard A (1987) Membrane impedance of internodal cells of *Chara corallina* obtained by analysis of low level transients. *Bioelectrochem Bioenerg* 17:131-139
- Homblé F, Ferrier J, Dainty J (1987) Voltage-dependent K^+ -channel in protoplasmic droplets of *Chara corallina*. A single channel patch clamp study. *Plant Physiol* 83:53-57
- Homblé F, Jenard A, Hurwitz HD (1988) Some techniques for investigation of electrochemical and ion transport properties of biological cell membranes: the case of *Chara corallina*. In: Dryhurst G, Niki K (eds) Redox chemistry and interfacial behavior of biological molecules. Plenum Press, NY
- Jorgensen PL (1975) Isolation and characterization of the components of the sodium pump. *Quart Rev Biophys* 7:239-274
- Kishimoto U (1961) Current voltage relations in *Nitella*. *Biol Bull* 121:370-371
- Kishimoto U (1974) Transmembrane impedance of the *Chara* cell. *JPN J Physiol* 24:403-417
- Marmarelis PZ, Marmarelis VZ (1978) Analysis of physiological system: the white-noise approach. Plenum Press, NY
- Ross S, Ferrier J, Dainty J (1985) Frequency-dependent membrane impedance in *Chara corallina* estimated by Fourier analysis. *J Membrane Biol* 85:233-243
- Segal JR (1967) Electrical capacitance of ion-exchanger membranes. *J Theor Biol* 14:11-34
- Singer SJ, Nicolson GL (1972) The fluid mosaic model of the structure of cell membranes. *Science* 175:720-731
- Smith PT (1984) Electrical evidence from perfused and intact cells for voltage-dependent K^+ channels in the plasmalemma of *Chara australis*. *Aust J Plant Physiol* 11:303-318
- Vorobiev LN, Musaev NA (1979) Electrical characteristics of the cell wall and plasmalemma of *Nitellopsis obtusa*. Low frequency impedance. *Sov Plant Physiol* 26:570-577

Image Instrumentation Methods of Plant Analysis

K. OMASA

1 Introduction

Knowledge and understanding of the biological world result from information about organisms and their interactions with their surroundings. Although information can come from many sources, tremendous advances in science have occurred with advances in instrumentation and technology, e.g. microscopes. Recent advances in electronics have greatly increased the amount of information that can be obtained. The development of image instrumentation technology which gather two- or three-dimensional information about the organism in non-destructive manner, has been particularly remarkable. In the field of medicine instrumentation technologies for surface, microscopic, X-ray, RI (radio isotope) and ultrasonic images have been put to practical use for patient diagnoses. In conjunction with advances in computed tomography (CT), tomographic images that give not only morphological information but also functional and physiological information have also been obtained (Herman 1979; Onoe 1982; Mansfield and Morris 1982).

In the field of plant research, a variety of image instrumentation technologies similar to those in the field of medical science, have been developed for cell individual plants, and small-scale plant communities (Omasa and Aiga 1988; Omasa et al. 1988). These technologies are used to elucidate the reaction mechanisms of living plants in fields such as physiology and physiological ecology. Based on the information obtained from these fundamental studies, diagnosis of plant growing conditions, injury by disease and pests, nutrition disorders, and environmental pollution injury, etc., have become possible. In addition, in the field of biotechnology these technologies can also be used for screening plants obtained by such methods as breeding, cell fusion, and gene recombination.

Development of wide-area remote sensing for plant communities by artificial satellites or airplanes has also been quite remarkable (Colwell 1983). The sensing is used to survey cropping acreage of fields, to estimate yields, and also to investigate changes in vegetation and ecosystems. Since a TM (Thematic Mapper) with many spectral bands and about 30 m resolution has been mounted in Landsat, the expansion in applications of remote sensing to agriculture or vegetation investigation are expected. However, wide-area remote sensing for large-scale plant communities are limited in terms of physiological information obtained from living plants. Therefore, in order to extend the applications, image instrumentation technologies for individual plants and small-scale plant communities which will combine physiology at the cell level with information obtained from the wide-area remote sensing, are important.

The application fields for image instrumentation of living plants include those of the future, listed in Table 1. The instrumentations are expected to be used in great many fields, ranging from the fundamental to the applied, such as botany, agriculture, environmental science, space science, and pedagogy.

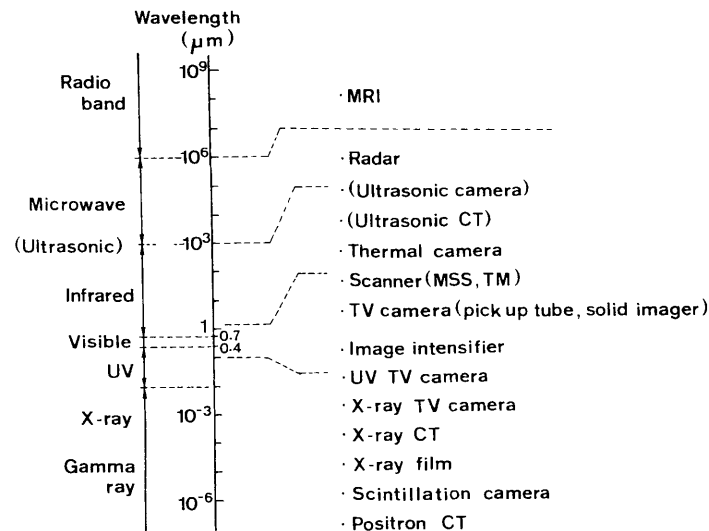
Table 1. Major application fields for image instrumentation of living plants

- * Diagnoses of injury by diseases and pests, nutrition disorders, environmental pollution injury, etc.
- * Plant growth monitoring and culture control
- * Biotechnology (mainly screening)
- * Automatization of farm work (robotics)
- * Diagnoses of environmental purification capacity
- * Educational systems for plant diagnoses and culture control
- * Auxiliaries for wide-area remote sensing
- * Other research in fields such as physiology, ecology, agriculture, environmental science and space science

2 Image Sensor Selection and Processing System

2.1 Image Sensor and Plant Information

Human eyes perceive only a very narrow band (visible rays) of the electromagnetic spectrum and limit the information obtained. In image instrumentation and wide-area remote sensing, however, information that cannot be obtained simply through human eyes can be obtained by using sensors capable of detecting electromagnetic (or sound) waves of various bands, and high-sensitivity sensors. Figure 1 shows the wavelength of electromagnetic (or sound) waves and typical sensors used in the respective bands.

**Fig. 1.** Wavelength of electromagnetic (or sound) waves and typical image sensors

One requirement for actual instrumentation using these sensors is the presence of electromagnetic waves for the active or passive bearing of information about objects. Active instrumentation methods, in which electromagnetic waves are irradiated to obtain information from living plants, have been developed recently, as an addition to the passive method, which uses only electromagnetic waves from the environment. Active instrumentation method features selective acquisition of information on specific physiological and biochemical reactions, but it has the disadvantage of exerting influence on the plant environment. The information such as minute area, internal conditions, and metabolic processes of the living plants is obtained by combining such techniques as RI, microscopes, and CT. Plant information and to appropriate image instrumentation apparatuses are listed in Table 2. The list includes techniques developed for medical or industrial use, which are applicable to the plant field, in addition to those developed specifically for plant research. Typical image instrumentation methods for obtaining plant information are described in detail in Section 3 and thereafter.

Table 2. Plant information and to appropriate image instrumentation apparatuses

Plant information	Image instrumentation apparatus
* Growth, shape, community structure	Multispectral camera (TV, scanner), stereo or moire camera, ultrasonic camera, CT (X-ray, NMR, ultrasonic)
* Plant temperature, transpiration, gas absorption	Thermal camera (including scanner)
* Stomatal response	Thermal camera, remote-control light microscope system
* Photosynthetic system, activity	High-sensitivity spectral camera
* Visible injury, plant pigment, color and luster	Multispectral camera (TV, scanner)
* Cell, organelle	Light microscope system
* Structure, physiological function inside organism (e.g., annual ring, rot, water content, transfer and metabolism of organism components)	CT (X-ray, NMR, ultrasonic, positron), X-ray TV camera, scintillation camera

2.2 Image Processing System

The amount of data obtained by image instrumentation is huge. For example, think about displaying a color photograph as digital images of red (R), green (G), and blue

(B). In order to obtain an image quality as good as that of the original seen only with the eyes, the amount of information required is above 512×512 pixels and 256 gradations in each digital image. If this amount is expressed by bytes, a unit used in computers, it is about 786 KB, corresponding to almost the total capacity of one floppy disc, as used for personal computers. If the object is a three-dimensional and moving image, the amount of information handled greatly increases. Recent advances in computer technologies, represented by 32-bit super personal computers, array processors, and optical discs with large-capacity memory are outstanding and complicated calculations that until now have only been possible using large-scale computers can now be carried out using portable image processing systems. Packages of image processing software with good compatibility, such as SPIDER (Kyodo System Kaihatsu, about 700 subroutines of FORTRAN 77 if SPIDER-II is included) have also been sold on the market.

As an example of a portable high-speed image processing system, our system is shown in Fig. 2. This system consists of a super personal computer (MASSCOMP MC 5400) with an array processor for floating point operations, a color graphic display (KRC, nexus 6800) with simple functions for image processing, and an optical disc unit of the write-once type (Matsushita Denso CU-15, DU-15), with a large capacity for image recording.

The MC5400, used as the host computer, is a small light-weight computer with a 32-bit virtual CPU (central processing unit) based on Motorola's MC 68020 (16.7 MHz) and uses UNIX (AT&T System V + Berkeley 4.2BSD), with real-time operating functions as the OS (operating system). Many languages such as C, FORTRAN 77, Franz LISP, Common LISP, and Prolog are applicable, and the

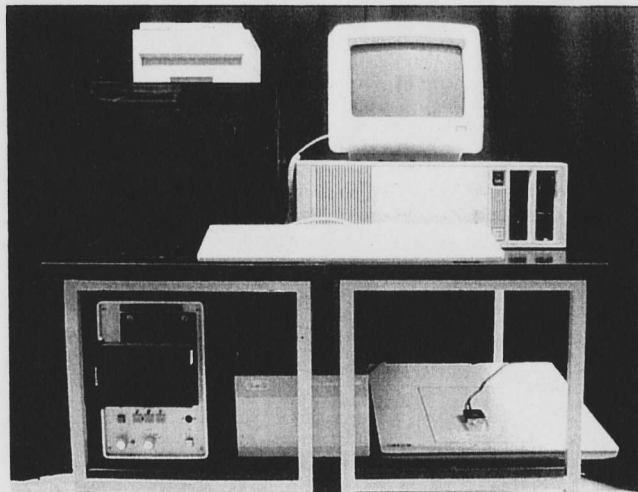


Fig. 2. Portable high-speed image processing system

software compatibility is good. For high-speed processing of floating-point operations, required for image processing, the system has a double precision high-speed processor by pipeline processing (FPA-1; 0.6 Linpack MFLOPS; 3.5 MWhets/s) and a single precision array processor of the built-in type (VA-1; 14 MFLOPS), in addition to a standard MC 68881 (0.1 Linpack MFLOPS; 1.1 MWhets/s). In particular, the array processor has approximately 250 libraries and can carry out, for example, addition and multiplication of 1024 points in $160 \mu\text{s}$ and complex FFT in 4.5 ms. Due to this capacity, the system realizes a processing speed from several times to some tens times faster than that of a system with only an MC 68881, and can process complicated operations such as CT reconstruction.

The color graphic display with eight frame memories ($512 \times 512 \times 8$ -bits) is capable of displaying any three frame memories as a color image (approximately 16.7 million colors; RGB each 8 bits), and also has functions such as zooming, and plotting. The graphic display can also attain various processings required for display, such as image smoothing, space filter, and addition/subtraction/multiplication between frame memories and segmentation, in 1/30 to several seconds using an 8- or 16-bit integer image processor of the built-in type. Since this processor has a processing speed from several to several hundred times faster than that of general purpose personal computers, it is able to carry out simple image processing on its own. The host computer and the graphic display are connected by a GP-IB bus (100KB/s) in order to send and receive data and control commands. Image data is digitized by a high-speed image A/D converter connected to the display, if the image signal is an RGB or NTSC type. If it is another type of image signal, it is digitized by a multipurpose high-speed A/D converter connected to the host computer. For example, a TV image can be digitalized in 1/30 of a second, and preprocessing such as noise removal, shading correction, and density level conversion can be executed in real time by the processor built into the display.

The optical disc unit connected to the graphic display is used to store the image data. One optical disc (1.2GB) can store approximately 5000 digital images ($512 \times 480 \times 8$ bits). It can write (2.7 s) and read (1.4 s) between the optical disc and the display at high speed. With its tree structure, the directory makes it easy to edit the files for an image data base. Due to remarkable advances in optical disc technologies in recent years, practical and erasable devices will be marketed in the near future. A combination of technologies for optical read-only discs will allow the spread of inexpensive image data bases.

The high-speed image processing system described above is still costly, although computers and graphic displays have become inexpensive. However, 32-bit work stations have recently become popular and inexpensive, and can be purchased for about one million yen. The work station transplanted SPIDER may serve almost all purposes if one is not overly concerned with processing speed and the number of colors displayed. Due to advances in VLSI technologies, single-chip real time signal processors with capacities equivalent to that of array processors have become commercially available. In the near future, high-speed image processing systems will also be available cheaply and will become personal systems in fact as well as in name.

3 TV Spectral Image Instrumentation

Since spectral reflection, transmission, and absorption properties of plants in wavelength from near ultraviolet to near infrared (0.3 to 2 μm) are influenced by such factors as surface or internal structure, type and amounts of plant pigments, and water conditions, they are important as plant information (Gates et al. 1965; Myers 1983). Particularly in the band below 0.8 μm , plants are known to absorb light and emit fluorescence in relation to physiological reactions such as photosynthesis, photomorphogenesis, and stomatal reactions (Trebst and Avron 1977; Kendrick and Kronenberg 1986; Sharkey and Ogawa 1987). This band sensed by human eyes is important for obtaining information on characteristics of plant growth such as shape, community structure, and visible injury. The TV spectral image instrumentation method is used to obtain plant physiological information or growth characteristics using TV spectral cameras with various optical filters (a special one is a color camera by RGB synthesis), and by using cameras according to the stereo or moire method. Movement of a stoma and morphological or physiological information at the cell level can be obtained by a light microscope with the high-sensitivity camera (See Sect. 4). Techniques for measuring chlorophyll fluorescence transients with information of photosynthetic system will be described in Section 5.

3.1 Types and Features of TV Cameras

TV cameras with image pickup tubes and solid imagers for detecting bands from near ultraviolet to near infrared have been placed on the market. Pickup tube cameras have a variety of spectral sensitivities in the range of 0.2 to 2 μm , resolution, dark current, and after-image. The image distortion, image stability, and shading are automatically corrected by electric circuits in the camera. The solid camera has also been developed as a next generation camera and a substitute for the pickup tube camera. Cameras with solid imagers (sensitivity range; 0.4 to 1.1 μm) such as CCD (charge coupled device) and MOS (metal-oxide-silicon) have recently been marketed. Color cameras of broadcasting standard are now becoming available as well, and these solid cameras are expected to be small in size and light in weight, to work at low voltage and low power consumption, to be highly reliable, and to have a long service life. The resolution, however, is usually worse than that of pickup tube cameras. They are also characterized by the lack of image distortion and burning, and the decrease of after-images. For instrumentation under very weak light, the use of a SIT (silicon intensifier target) camera and the mounting of an image intensifier are required.

The household VTR is often used to record color or black-and-white images for image analysis. However, if high image quality and time code accuracy are required, VTRs of broadcasting standard with time base correctors and time code recording functions are more suitable, although they are expensive. Optical disc devices for recording TV images are commercially available, although they are also expensive.

3.2 Spectroradiometer for Field Measurement

The selection of TV camera and optical filters requires a knowledge of the spectral properties of the light environment and subject. A portable spectroradiometer (Omasa et al. 1982) and a standard light source for calibration are shown in Fig. 3.

The analyzer consists of two diffraction grating spectroscopes for scanning a range of 0.250 to 0.900 μm (Ch 1: photomultiplier R636 is used as a detector) in 1 s and a range of 0.850 to 2.50 μm (Ch 2: PbS cell) in 5 s, and a signal processor to control the spectroscopes and to analyze the measured data. The detector is electronically cooled to improve the sensitivity and S/N. The wavelength resolution and the stray light are ± 1 nm at Ch 1, ± 3 nm at Ch 2, and 1×10^{-4} . Light is introduced from a condenser or an integrating sphere attachment (Fig. 4) to the spectroscopes via optical fibers. The condenser is used to measure the spectral reflection properties of a subject far away (0.8 to infinity m), and the attachment is used to measure the special reflectance and transmittance by the built-in light source and integrating sphere.

The signal processor is an interactive system with a CRT (cathode ray tube) display for data collection and analysis. The measured data are automatically calibrated based on the verification value of the standard light source and are stored in a magnetic cassette tape. Since the signal processor has functions of continuous addition and collection of data when a subject is measured under very weak light, it can expand its dynamic range for the quantity of light in combination with the selection of slit width for the spectroscopes. In addition, the processor has additional

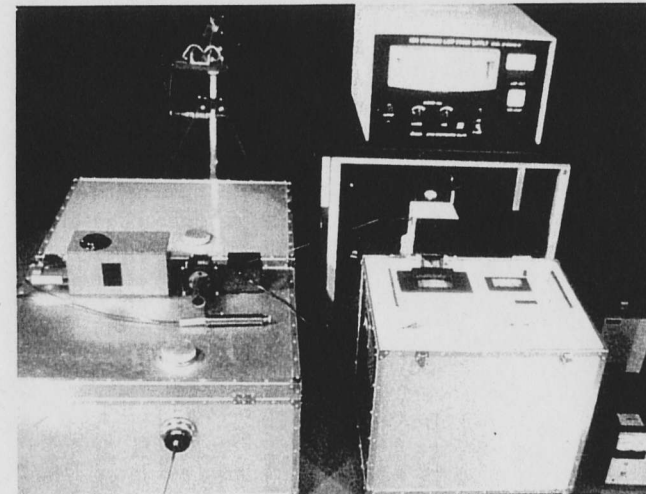


Fig. 3. Portable spectroradiometer and standard light source for calibration



Fig. 4. Attachment with light source and integrating sphere for introducing light to spectroscopes via optical fibers

functions such as four arithmetic rule operations between measured data, multiplication of coefficient, and calculation of energy in a specified band.

Spectral reflectances of the healthy part and the visibly injured part of plant leaves measured using the integrating sphere attachment are shown in Fig. 5. In the healthy part, the reflectance below $0.7 \mu\text{m}$ becomes smaller due to absorption by plant pigments, and in $1.4 \mu\text{m}$ ($1.9 \mu\text{m}$ absorption band is impossible to measure) it becomes smaller due to water absorption. However, in the visibly injured part of the leaf (in a dry state), the reflectances of these bands are large. In the non-dried state, the absorption by water in the near infrared band remains. An optical fiber of UV grade is used for Ch 1, and one with no absorption by water in the near infrared is used for Ch 2. Measurements using this attachment are limited to the band between 0.4 and $1.8 \mu\text{m}$ because of the spectral properties of the light source energy (tungsten halogen lamp), optical fiber transmission, and integrating sphere reflection in addition to sensitivity of detectors. Spectral reflectance and transmittance can be measured within an error margin of about 3%. On the other hand, the condenser allowed the measurement of the band from 0.25 to $2.3 \mu\text{m}$.

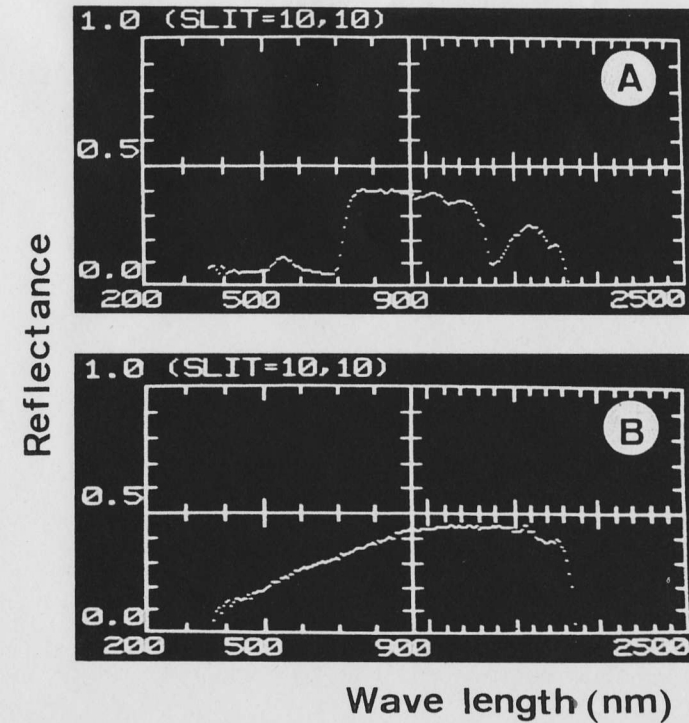


Fig. 5. Spectral reflectances of leaves measured using the integrating sphere attachment. A Healthy part; B visibly injured part

3.3 Image Instrumentation of Plant Growth and Shape

Plants grow because of cell division and cell elongation. The growth speed differs by location and changes at each growing stage. Therefore, it is important to investigate spatial differences and changes over time in the growth rate of plant organs. The important problem in growth instrumentation is distinguishing the objective organs from the background. Plant reflectance is larger in the near infrared band of 0.8 to $1.3 \mu\text{m}$ in comparison with that of the background soil (Myers 1983). Therefore, the plant community growing in the soil is easily extracted by near infrared spectral images, although some parts remain hidden because of surface instrumentation. The community growth characteristics such as leaf area, leaf area index, dry weight, and plant height are estimated from calculations of matrix elements of binary images extracted by measuring a community from multiple directions (Matsui and Eguchi 1978). Also, it is possible to estimate, although not very accurate, the characteristics of community growth by measuring the intensity of reflected light from plant community.

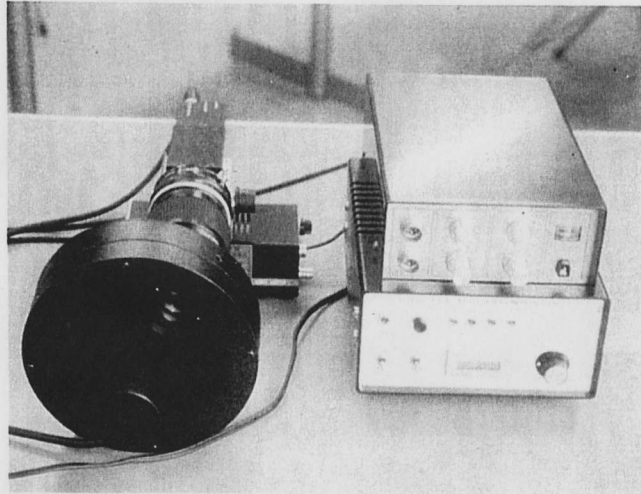


Fig. 6. Multispectral TV camera with 4-band rotary attachment

A multispectral TV camera developed by the author for image instrumentation of plant growth and visible injury is shown in Fig. 6. A rotary attachment with an automatic function for the changing filters is attached to the front of a TV camera, thus allowing spectral images to be made at four different wave bands. The combination of image pickup tube (or solid imager) and optical filters is selected depending on the purpose. For plant instrumentation, a typical combination is a silicon vidicon tube (or a CCD imager) camera with sensitivity in the band of 0.4 to 1.1 μm and interference filters whose central wavelengths are 0.45, 0.55, 0.67, and 0.90 μm (half-bandwidth: 0.01 to 0.03 μm).

Figure 7A shows a spectral image in the near infrared band (0.90 μm) of a sweet potato plant community growing in the field. The use of spectral image allows the separation of the plant community from the background by thresholding (Fig. 7B). The spectral image instrumentation is an effective method for extraction or growth analyses of the leaf, petal, fruit, and other organs.

Although stereo and scanning moire methods using TV cameras permit the measuring of simple three-dimensional shapes, it is impossible to obtain information such as the intricately shaped inside structure of plants and roots in the soil. These subjects must be measured by other methods such as CT.

3.4 Image Instrumentation of Visible Leaf Injury

Necrotic and chlorotic visible leaf injury is caused by the destruction of leaf tissue and the loss of plant pigments. The reflectance of a healthy leaf at wavelengths below 0.7 μm is small, due to absorption by plant pigments such as chlorophylls and

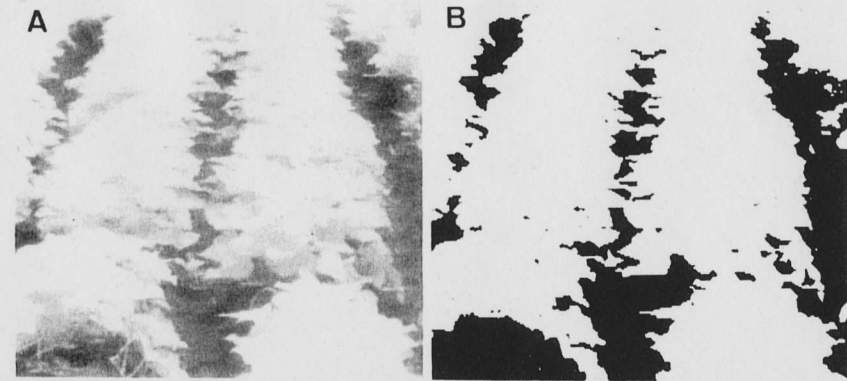


Fig. 7A,B. Spectral image of sweet potato plants growing in the field and their areas extracted by thresholding. A Spectral image (0.9 μm); B two-valued image; white is plant area and black is soil area

carotenoids (see Fig. 5). However, in the visibly injured leaf, the reflectance becomes greater, due to the loss of plant pigments. Figure 8 shows two types of typical visible injuries. One features numerous, discrete and unclear injuries, and the other features broad and clear injuries.

Spectral image analysis provides two objective methods for evaluating these visible injuries (Omasa et al. 1983a, 1984). One method uses the average gray level or band ratio obtained from the spectral image as an index for the evaluation. Table 3 shows the correlation coefficients and standard errors which indicate the relationship between the total chlorophyll content, which is a major component of the lost pigments, and the average gray level or band ratio of their spectral images measured through various interference filters (central wavelength 0.45, 0.55, 0.67, 0.78, 0.90 μm with respective half-bandwidth 0.03, 0.01, 0.01, 0.01, 0.01 μm) under constant lighting with a silicon vidicon camera. The correlation is the highest in the case of a band ratio of 0.55/0.90, where the correlation coefficient is -0.95 . The standard error in evaluating the total chlorophyll content under this band ratio is 4.2

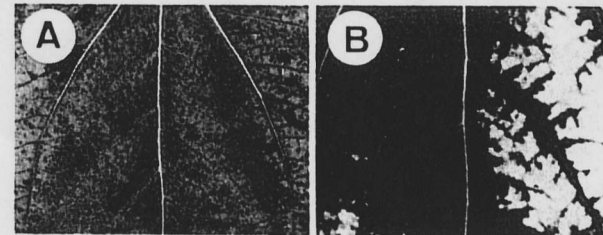


Fig. 8A,B. Two types of typical visible injuries. A O_3 injury; B SO_2 injury (Omasa et al. 1984)

Table 3. Correlation coefficients and standard errors which indicate the relationship between the total chlorophyll content and the average gray level or band ratio of various spectral images (Omasa et al. 1983a)

Wavelength of image or band ratio	Correlation coefficient	Standard error
0.45 (μm)	-0.91	5.6 ($\mu\text{g cm}^{-2}$)
0.55	-0.89	6.1
0.67	-0.87	6.7
0.78	-0.09	
0.90	0.03	
0.45/0.90	-0.93	5.1
0.55/0.90	-0.95	4.2
0.67/0.90	-0.88	6.4
0.78/0.90	-0.20	
0.45/0.78	-0.91	5.7
0.55/0.78	-0.91	5.8
0.67/0.78	-0.86	6.9
0.45/0.67	0.16	
0.55/0.67	0.60	10.9
0.45/0.55	-0.78	8.5

$\mu\text{g cm}^{-2}$. This method is especially effective for the evaluation of numerous, discrete, and unclear injuries, such as O_3 injury.

The other method uses the ratio of the injured area to the leaf area. The most effective wavelength of the interference filter for separating the injured part from the healthy part is $0.67 \mu\text{m}$, because the difference between the average gray levels of these parts in the spectral leaf image is the greatest. This method is effective for the evaluation of broad and clear injuries, such as SO_2 injury. The complex injury caused by mixed pollutants, pathogenic fungi, noxious insects, etc., can be evaluated by the combined use of both methods.

Also, since the reflectance in $1.4 \mu\text{m}$ and $1.9 \mu\text{m}$ depends on the water content of the plant tissue, the spectral image of these bands provides information relating to the severe drying out of visibly injured leaves (Knipling 1970; Myers 1983). However, a slight change in water content or the water potential of a healthy leaf is not detected by the spectral image.

4 Remote-Control Light Microscope System

In many research fields of biology, the optical light microscope is widely used to observe plant tissues and cells. The use of a TV camera and monitor instead of the naked eye facilitates observation. The use of an image processor for analyzing signals from the camera also makes it possible to evaluate cell growth, the shape of organelles, their color tones, etc. The SIT camera and image intensifier are used effectively to observe them under weak light.

Direct observation of the stomatal movement of attached leaves had been very difficult under the plant's actual growing conditions (Meidner and Mansfield 1968; Meidner 1981). Although the scanning electron microscope (Shiraishi et al. 1978) and the light microscope, in which a piece of leaf is immersed in water or liquid paraffin (Monzi 1939; Stålfelt 1959; Meidner 1981), can provide a clear image at high magnification, observation of intact stomata under their growing conditions is impossible. Observation with an ordinary light microscope under a plant's growing conditions poses some problems (Heath 1959; Meidner and Mansfield 1968); first, visual observation under weak light is very difficult; second, the environment of the lower side of the leaf cannot be controlled, because the leaf is directly held on the microscope stage, and the environment is also affected by human manipulation of the microscope; and third, the working distance, that is, the distance between the leaf and the objective during the observation, is very small at high magnification, thus subjecting the leaf to the danger of sticking to the objective during focusing and destroying the environment between the leaf and the objective. Omasa et al. (1983b) and Kappen et al. (1987) have solved the above problems of the ordinary light microscope. As an example of a light microscope system coupled to an image processor, our system for the measurement of stomatal movements of attached leaves under actual growing conditions is introduced in this section.

4.1 Outline of the System and Its Performance

Figure 9 shows our remote-control light microscope system. This system has a light microscope (Bausch & Lomb, MicroZoom) with a wide working distance (ca. 13 mm) at high magnification (a 50x objective, 1.5x and 2x amplifiers and a TV adapter lens; ca. 1600-fold magnification on a TV monitor), an SIT video camera (Hamamatsu TV, Model C1000-12) with high sensitivity S20 type spectral response, image resolution of over 600 TV lines, distortion within 2% and shading within 20% as a detector of the microscope image, a monochromatic TV monitor (Chuomusen, Model MD2002A) with image resolution of ca. 1000 TV lines and distortion within 3% and remote controllers for adjusting camera sensitivity, a microscope focus, and movement of the microscope stage in a separate room. The microscope images are projected on the TV monitor in a separate room and recorded photographically on black-and-white (B & W) film or by a VTR (SONY, BVU820) (horizontal resolution, 340 TV lines at B & W mode; S/N, ca. 50dB) with a digital time base corrector (SONY, BVT800) and a time code generator/reader. The image processing for evaluating stomatal aperture and cell injury is carried out by a system composed of a high-speed video processor, graphic displays, and a host computer (See Sect. 2.2).

Figure 10 shows a schematic cross-sectional view of the microscope stage designed to hold the leaf of an intact plant. The leaf (C) is held on a ring (F, 30 mm in inner diameter, 10 mm wide and 10 mm high) fixed to a remote-control movable stage (G) by a holding ring (E, the same diameter and width as F, 3 mm in height), in order to have the conditioned air pass under the surface of the leaf. Furthermore, since the center of the movable stage is cut to a circle 30 mm in diameter, and the distance between the movable stage and plate (H) fixed on base (K) is kept at 10 mm,

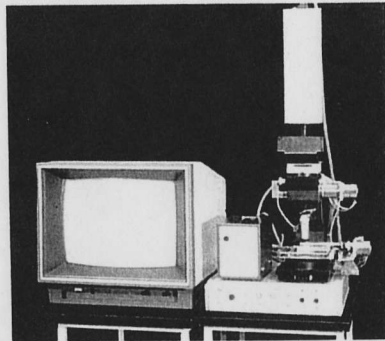
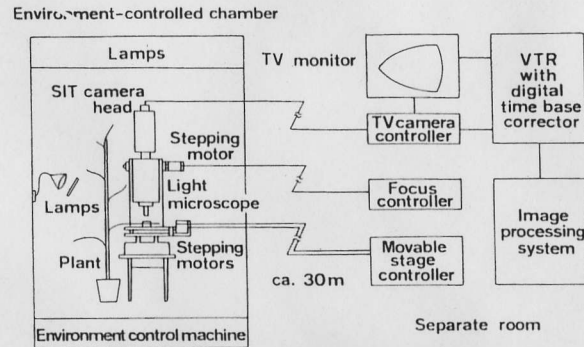


Fig. 9. Remote-control light microscope system (After Omasa et al. 1983b)

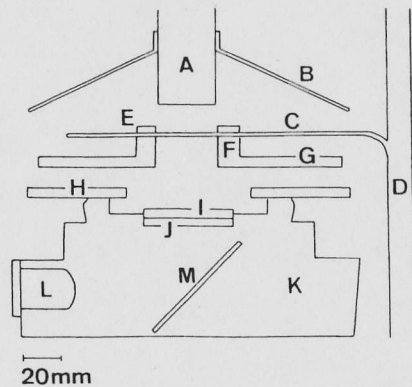


Fig. 10. Schematic cross-sectional view of the microscope stage for holding an intact leaf. *A* Objective; *B* shade cover; *C* leaf; *D* stem; *E* holding ring; *F* ring fixed to remote-control movable stage; *G* remote-control movable stage; *H* plate; *I* heat-absorbing glass filter; *J* diffusing filter; *K* base; *L* halogen lamp; *M* mirror (Omasa et al. 1983b)

the same temperature and humidity can be maintained on both sides of the leaf. The movable stage and the plate are made of transparent acrylic resin, to allow light from the environment to enter. The shade cover (*B*) is not used except for observation with transmitted light. Although observation is usually carried out with light from the environment, a halogen lamp (*L*) is sometimes used as a supplementary light source for observation with transmitted light.

Figure 11 shows photomicrographs of an intact stoma observed with reflected and transmitted light using the remote-control light microscope system. The stomatal image was clear at high magnification (ca. 1600-fold magnification on the TV monitor). The stoma was observed with reflected light and then rapidly observed with transmitted light, and the stomatal aperture was found to be the same for both. Although this system could provide stomatal images with a mixture of reflected and transmitted lights, the clearest images were obtained with either reflected or transmitted light alone. The stomata could be observed with either reflected or transmitted light above ca. 0.1 mWcm^{-2} [environment illumination; ca. 2 klx (0.5 mWcm^{-2}) with reflected light, ca. 0.5 klx (0.5 mWcm^{-2}) with transmitted light]. If the observation with a single light of 0.1 mWcm^{-2} is done with the naked eye through the eyepiece instead of the SIT camera, the eye must be sufficiently acclimatized to the dark room. The attachment of an image intensifier to the SIT camera produces a further increase in sensitivity, although the image quality becomes poor. Although the resolution of the microscope image was within $1 \mu\text{m}$, it is improved by a digital image processing technique. Omasa and Onoe (1984) were able to evaluate the stomatal aperture within $0.3 \mu\text{m}$ standard error using this technique, even when the microscope image was of poor quality.

4.2 Continuous Observation of Guard and Epidermal Cells

When the light microscope system was used for continuous observation of the stomatal movement of an intact growing plant, we obtained photomicrographs

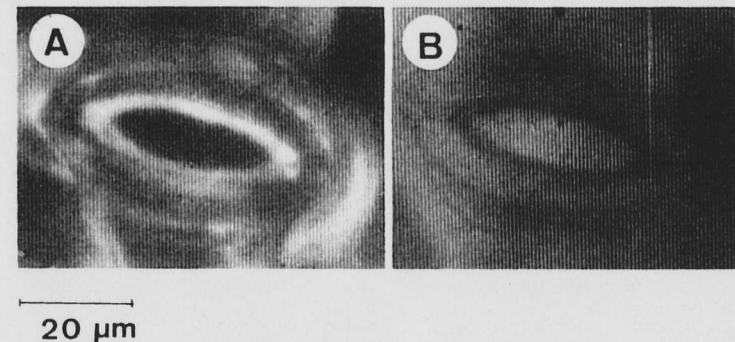


Fig. 11A,B. Photomicrographs of an intact sunflower stoma observed with reflected or transmitted light using the light microscope system. *A* Reflection image; *B* transmission image (Omasa et al. 1983b)

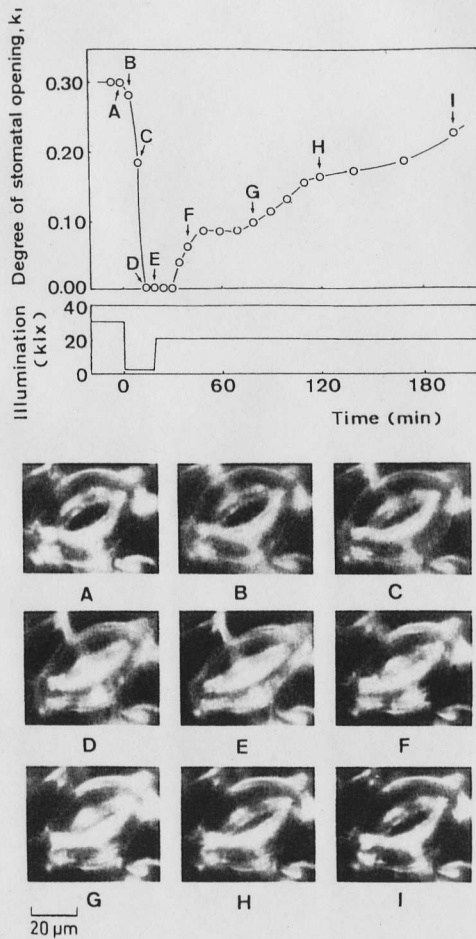


Fig. 12. Responses of an intact stoma of the adaxial epidermis of a broad bean plant to illumination changes; k_1 is the degree of stomatal opening expressed by the ratio $l_a/l_{b_{max}}$, where l_a is the width of the stomatal pore and $l_{b_{max}}$ is the maximum length of the fully opened stomatal pore. Photomicrographs (A-I) correspond to time points (A-I) in the k_1 change. The illumination was changed from 30 to 2 klx at 0 min (A) and from 2 to 20 klx at 20 min (E). Other environmental conditions: air temperature, 20.0°C; RH, 70% (Omasa et al. 1983b)

similar to those in Fig. 12, which show the response of an intact stoma of the adaxial epidermis of a broad bean plant to an illumination change. The illumination was changed from 30 klx (11.9 mWcm⁻²) to 2 klx (0.5 mWcm⁻²) at 0 min (A) and from 2 to 20 klx (7.7 mWcm⁻²) at 20 min (E). The movement of the central pore of the stoma could be continuously observed; the degree of opening (k_1) of the stomatal

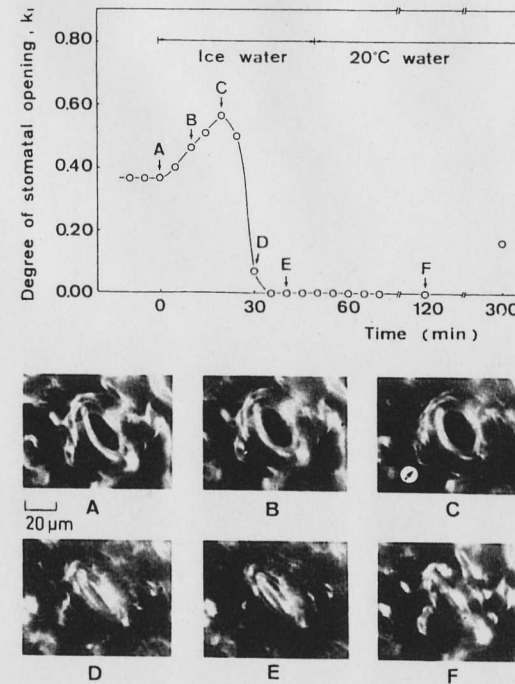


Fig. 13. Responses of an intact sunflower stoma to water deficit. The water deficit was caused by ice water perfusion to roots. Photomicrographs (A-F) correspond to time points (A-F) in k_1 change. The arrow (A) in C shows first hollow of subsidiary cell. Environmental conditions: air temperature, 25.0°C; RH, 60%; light intensity, 600 $\mu\text{mol photons m}^{-2}\text{s}^{-1}$ (Omasa and Maruyama 1990)

pore is expressed by the ratio $l_a/l_{b_{max}}$, where l_a is the width of the stomatal pore and $l_{b_{max}}$ is the length of the fully opened stomatal pore. The stoma began to close within 5 min (B) of lowering the illumination (30 to 2 klx) and became completely closed after ca. 15 min (D). It began to reopen within 15 min of raising the illumination (2 to 20 klx), and after 180 min (I), had recovered to ca. 75% of aperture before the illumination change.

Figure 13 shows changes in an intact sunflower stoma as a result of water deficit caused by ice water perfusion to its roots. The stoma increased its aperture within a few minutes of perfusion and reached a maximum opening at 20 min (C). Thereafter, it began to close and reached complete closure at 35 min (E). Subsidiary cells observed in the photomicrographs began to become hollow at ca. 20 min (C) and then the hollow expanded from the epidermal cell to the guard cell (C to E). The transient opening from "A" to "C", therefore, may be caused by the rapid decrease in subsidiary cell turgor in comparison to guard cell turgor, due to a decrease in water uptake from the root. After 20°C water perfusion, the cell form slowly recovered (F) and the stoma began to reopen ca. 3 h later.

Figure 14 shows the varying responses of the stomata to 1.5 $\mu\text{mol SO}_2$ at the border of the injured region near a veinlet. These stomata continued to maintain constant apertures until about 15 min after the start of the exposure, when a wide variety of stomatal responses began. Stomata in area I contiguous to the veinlet

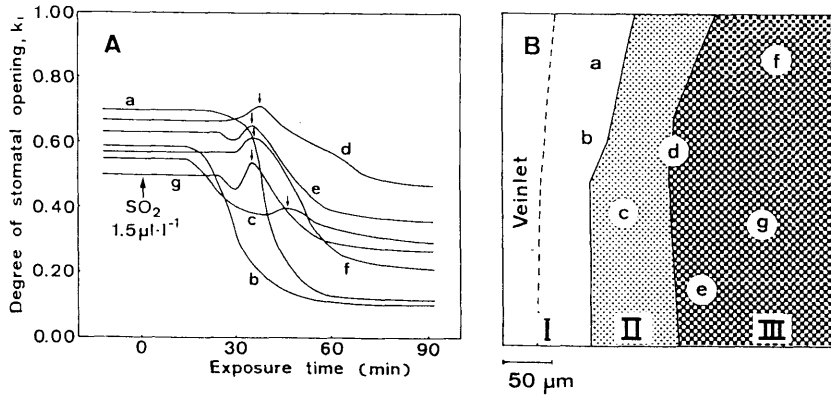


Fig. 14. Responses of neighboring stomata to $1.5 \mu\text{l l}^{-1}$ SO_2 at the border of an injured region near a veinlet. **A** Stomatal responses; *small arrows (t)* show when water soaking and cell collapse began to appear. **B** development of injury at the region; *I* uninjured region; *II* injured region where only cell collapse appeared, without water soaking; *III* injured region where both water soaking and cell collapse appeared. Environmental conditions: air temperature, 25.0°C ; RH, 60%; light intensity, $600 \mu\text{mol m}^{-2} \text{s}^{-1}$ (Omasa et al. 1985a)

showed rapid and continuous closure, and the guard and epidermal cells maintained normal turgor. Stomata in area III, at a distance from the veinlet, had a transient opening after either the closing or the keeping of a constant aperture, because of the rapid decrease in subsidiary cell turgor in comparison to guard cell turgor, caused by the appearance of water-soaking and cell collapse in the epidermal cells. The stomata then closed as the injury expanded to all cells. In area II, cell collapse occurred gradually without water-soaking from the cells near area III by the turgor loss of cells in area III. Therefore, the appearance of a transient stomatal opening in area II was later than that in area III.

Porometry or gravimetric measurements of transpiration do not provide the real aperture of stomata and the information for cell form and surface conditions (Omasa et al. 1985a). They also involve the risk of losing important information about the stomatal response, because they average the behavior of many stomata. Therefore, it is important to observe the individual stomata and their neighboring cells directly in order to examine the stomatal movement. Also, since this system is effective for observing many intact stomata because of its easy and rapid operation, it can be used to analyze the relationship between stomatal aperture and conductance under the plant's growing conditions.

5 Image Instrumentation of Chlorophyll Fluorescence Transients

Abiotic and biotic stresses such as air pollutants, water deficit, high or low temperature, and virus infection cause a spatially heterogeneous impairment in attached leaves. The invisible impairment was indicated in stomatal responses and photosynthetic activity. For example, recent investigations employing thermal imaging methods (See Sect. 6) and DLE (delayed light emission) imaging methods (Ellenson and Raba 1983; Ellenson 1985) have shown evidence of spatially different responses of stomata in situ to various stresses. The DLE imaging method, furthermore, clarified localized changes in photosynthetic activity induced by the stresses (Björn and Forsberg 1979; Ellenson and Amundson 1982). However, these techniques did not provide any information about the site of inhibition in the photosynthetic apparatus.

Rapid changes in intensity of chlorophyll *a* fluorescence during dark-light transition (CFI) reflect the various reactions of photosynthesis (Kautsky et al. 1960; Murata et al. 1966; Papageorgiou 1975), especially the photosynthetic electron transport system. Therefore, the measurement and analysis of CFI in plant leaves in situ has been developed as a sensitive and nondestructive assay for the functional state of the photosynthetic apparatus (Smillie and Hetherington 1983; Shimazaki et al. 1984; Sivak and Walker 1985). Recently, Omasa et al. (1987) developed a new instrumentation system using a CCD image sensor for a quantitative analysis of CFI, the system of which would give information not only about localized differences in photosynthetic activity on the whole leaf in situ but also about the inhibition site in the photosynthetic system. In this section, the system is introduced.

5.1 Outline of the System and Its Performance

Ordinary TV cameras and recording systems are not suitable for a quantitative analysis of CFI in attached leaves, because of their low sensitivity, large after-image, bad image quality, AGC (automatic gain control) function, and the indistinctness in timing of the playback image. Common tungsten and fluorescent lamps also cannot be used as light sources for CFI imaging, because of the unevenness and fluctuation in light intensity. The new image instrumentation system (Fig. 15) was designed to overcome these problems. A highly sensitive CCD imager with uniformity in sensitivity and an after-image suppression was selected for a TV camera (SONY XC-47, improved type). The image quality was improved by the use of a computer-control VTR (SONY BVU-820) with a digital time base corrector (SONY BVT-800) and the preprocessing by using a high-speed TV image processor (KCR nexus 6800). The AGC function, which changes a relationship between fluorescence intensity and the gray level of the recorded image, was removed from the TV camera and the VTR. The timing of the playback image was exactly defined by the use of a shutter synchronized to the TV signal and by the time code recorded in each image. The unevenness in light source intensity was improved by the use of two xenon lamp (CERMAX LX-300F) projectors, and by attaching a special ND filter with concentric circles of different density.

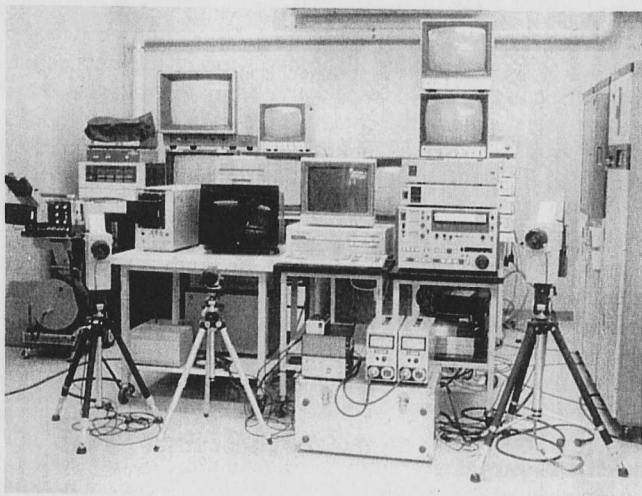
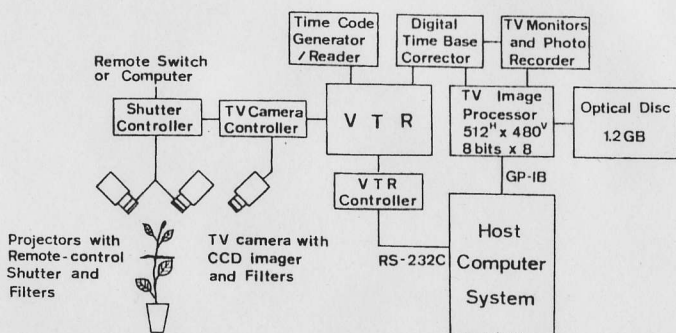


Fig. 15. Image instrumentation system for quantitative analysis of CFI in attached leaves (Omasa et al. 1987)

After the plant had adapted to the dark for 30 min, the CFI was provoked by irradiation of the whole leaf with two beams of blue-green light (380–620 nm) from the projectors, with band-pass filters via the shutter opening. The fluorescence image was continuously measured at a TV field interval of 1/60 s by the TV camera equipped with an interference filter (683 nm; half-band width, 10 nm) and a red cut-off filter (> 650 nm), and recorded, with time code, by the VTR. The VTR image was digitized by a video A/D converter after it was played back to a still image without guard band noise through the time base corrector. A series of the digitized images ($512H \times 480V$ 8 bits) was stored on an optical disc (National DU-15). A host computer system (MITSUBISHI MELCOM 70/40 and NEC PC9801 vm4) was used to control the VTR and TV image processor.

The CFI curves, intensity images of characteristic transient levels (I,D,P,S,M,T), and amplitude images of major transient characteristics (ID, DP, PS, MT) were calculated by the TV image processor on the basis of a series of images after preprocessing for shading correction and noise removal. These were indicated by scales which correspond to the A/D conversion level.

Figure 16 shows the relationship between the intensity of artificial light in the likeness of fluorescence and the A/D conversion level of VTR image. The data indicated a linear correlation between the light intensity and the A/D conversion level. Since the artificial light was sufficiently diffused, and the unevenness of the light intensity in the visual field of the TV camera was maintained within 0.1%, the standard deviation of 6.3% (maximum) in the A/D conversion level was due to image shading caused by unevenness in sensitivity of the TV camera and any noise other than VTR guard band noise. The image shading was corrected by calculating the ratio of an original image to a specific image (shading master), obtained by measuring a uniform light of definite intensity, because the shading was mainly caused by the lens and optical filters of the TV camera. The noise was removed by the use of a spatial smoothing filter, and the averaging of images digitized from a still VTR image. For example, the image quality could be improved to within 1% standard deviation by the shading correction and the smoothing of 3×3 pixels after an averaging of 10 images, when the image resolution was 280 lines. The after-image for the TV camera was about 4% at 30 ms after shutter opening, and decreased to 0.3% at 50 ms.

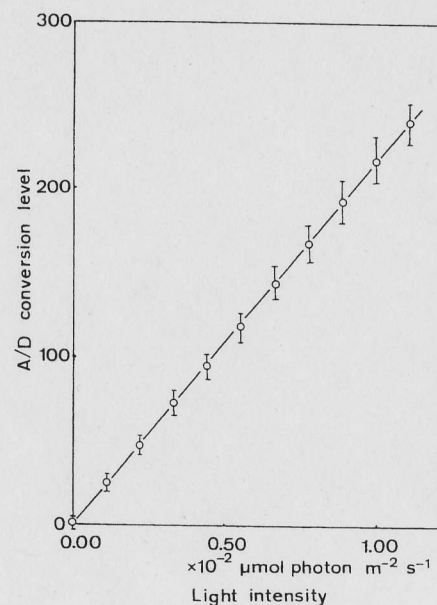


Fig. 16. Relationship between the intensity of artificial light in the likeness of fluorescence and the A/D conversion level of VTR image. Symbol \circ represents the mean value of A/D conversion levels of an image (512×480 pixels) measured at a light intensity and the vertical bar indicates \pm SD. The artificial light was sufficiently diffused and the unevenness of the light intensity in the visual field of the TV camera was maintained within 0.1%. The light intensity was measured by a quantum sensor through two filters placed in front of the TV camera (Omasa et al. 1987)

The CFI from a defined part of a cucumber leaf in situ was measured by our system under different intensities of actinic blue-green light. The CFI curves were calculated on the basis of a series of fluorescence images (Fig. 17). Those clearly revealed the typical IDPSMT transients (Papageorgiou 1975) under light intensities from 50 to 200 $\mu\text{mol photons m}^{-2}\text{s}^{-1}$ at leaf surface. In these intensity ranges of light, we could resolve IDPSMT transients from any part of the leaf surface which has an area of at least 1 mm^2 . Fluorescence intensities of I, D, P, S, M, and T, and rates in transients of DP, PS, and MT increased as the actinic light intensity increased. The appearance of peak P became more rapid with the increase of actinic light intensity.

Because the CFI is light intensity dependent, as described above, it is important to illuminate the whole leaf with uniform light when we want to compare CFI curves derived from different areas (each about 1 mm^2) of the leaf to the entire leaf. The combination of special ND filters and two projector lamps, which were placed at angles of 60° and 120° to the leaf surface, overcame this problem. The combination kept the spatial deviation of the intensity of actinic light within 5% over a flat surface of 20 cm in diameter.

Ellenson (1985) has reported a video recording system for DLE analysis, but its performance was not characterized. In general, the quality of DLE image is worse than that of chlorophyll fluorescence image, because the image intensifier was used to image DLE. The irradiation of a leaf with a tungsten projector lamp placed at an oblique angle to the leaf surface (Ellenson and Raba 1983) causes spatial differences in the intensity of actinic light. Moreover, it should be noted that the AGC function of the ordinary TV camera and VTR system changes a linear correlation between the intensity of DLE or CFI and the A/D conversion level.

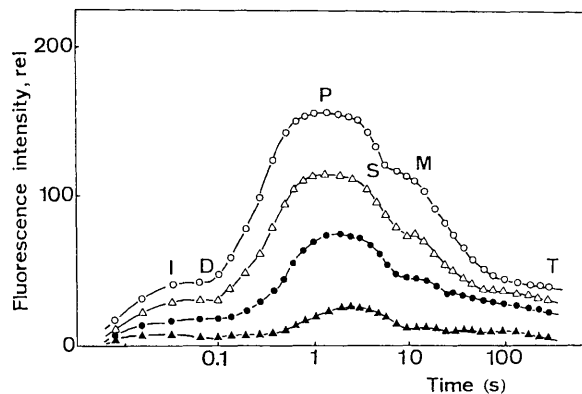


Fig. 17. The CFI curves of a small area (about 1 mm^2) of a healthy cucumber leaf in situ measured under different intensities of actinic blue-green light. Before measurement, the leaf was dark-adapted for 30 min. Intensity of actinic light (unit = $\mu\text{mol photons m}^{-2}\text{s}^{-1}$): (○) 200, (△) 150, (●) 100, and (▲) 50. Light intensities were varied using ND filters. Environmental conditions: air temperature, 25.0°C; RH, 70% (After Omasa et al. 1987)

5.2 Diagnosis of Photosynthetic System

The CFI image instrumentation system was used to diagnose the SO_2 effect on the photosynthetic apparatus (Omasa et al. 1987). Figure 18 shows the CFI curves and the images with a gray scale. In the unfumigated leaf area (UF), the CFI clearly showed the typical IDPSMT transients (Papageorgiou 1975) and almost identical transients at any location on the leaf area. Since the CFI observed upon dark-light transition of the leaf reflects the partial reactions of photosynthesis, we can detect the alteration in photosynthetic apparatus by SO_2 from the changes in CFI curves. As shown in Fig. 18, B and C, both the intensity images of characteristic transient levels (I, P, M, T) and amplitude images of major transient characteristics (ID, DP, PS, MT) in the fumigated counterpart (F) strikingly differed from those in the unfumigated area. Fluorescence intensity at I was raised and at P reduced markedly, and that at T was increased in the fumigated area. Amplitude of fluorescence transients of DP-rise and PS- and MT-decline, indicating photosynthetic activity, was reduced in the fumigated leaf. The changes in the intensity and amplitude varied with the location on the leaf surface; the effect of SO_2 was more severe in locations of interveins and veinlets than in those near large veins. Contrary to the perturbation in photosynthetic apparatus shown above, there was no visible injury on the whole surface of leaf at the end of SO_2 treatment and 2 days later.

The significance of the changes in CFI induced by SO_2 fumigation was as follows: Because fluorescence intensity in the early induction phenomena is regulated by the redox state of Q, a primary electron acceptor of PSII, the elevated I level suggest that some portion of Q was brought to a reduced state by the SO_2 -fumigation. Since the DP rise in CFI reflects the photoreduction of Q through reductant from H_2O , a diminished rise of DP was consistent with the inactivation of the water-splitting enzyme system. Since PS decline involves energy-dependent quenching, the suppression of PS decline suggested the depression of formation of *trans*-thylakoid proton gradient, probably due to the inactivation of the water-splitting enzyme system. However, the possibility that the PS decline was affected by the inhibition of electron flow Q to PSI cannot be excluded, because PS decline partly reflects the oxidation of Q by PSI. Suppression of MT decline was probably due to the inhibition of the *trans*-thylakoid proton gradient formation in addition to unidentified reactions in chloroplasts. Although the extent of the SO_2 -effect on CFI differed from area to area on a single leaf, the mode of SO_2 action was essentially the same.

The recovery from perturbation by SO_2 became evident by monitoring the CFI when the fumigated plants were transferred to SO_2 -free air (Fig. 19). Adjacent to the large midvein, where the alteration of CFI was relatively small, the CFI recovered completely and showed the IDPSMT transient identical to that of the unfumigated area. In most of the area near veinlets, the CFI which was affected strongly was also almost completely restored. However, the fluorescence emitted from the interveinal area was still affected during this period; the peak P reappeared but its intensity was still low, and the I level was elevated further. The elevated I level suggests that the irreversible injury to the PSII reaction center took place in chloroplasts. In contrast, the elevated T level in the quasi-stationary state became normal in this leaf area.

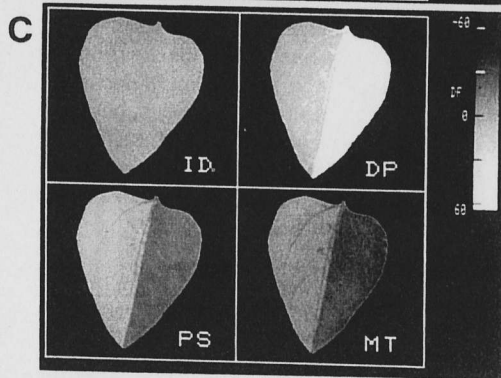
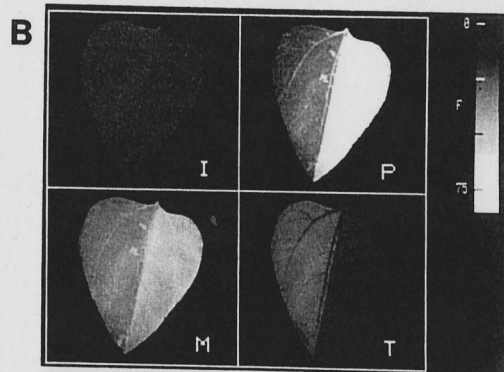
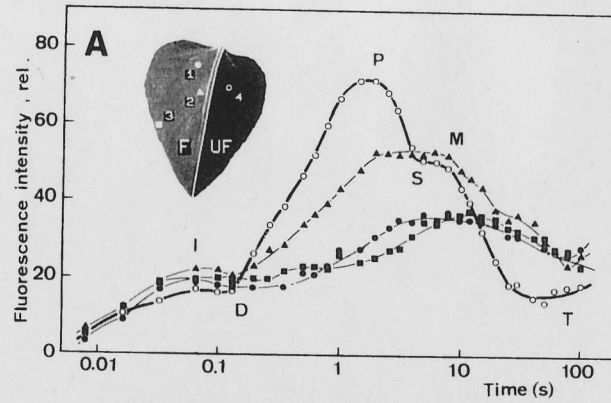


Fig. 18A-C. Effect of SO_2 on CFI in an attached sunflower leaf. Sunflower plant was fumigated with $62.4 \mu\text{mol SO}_2 \text{ m}^{-3}$ ($1.5 \mu \text{ l l}^{-1}$) at 25.0°C air temperature, 70% RH, and $350 \mu\text{mol photons m}^{-2}\text{s}^{-1}$ light intensity for 30 min. After dark-adaptation for 30 min, CFI of an attached leaf was measured under $125 \mu\text{mol photons m}^{-2}\text{s}^{-1}$ actinic light. **A** CFI curves at different sites in fumigated area (F: ● interveinal site 1; ▲ site 2 near a large vein; ■ site 3 near a veinlet) and unfumigated area (UF: ○ interveinal site 4). The vein and corresponding sites (1-4) are denoted in a photograph of the whole leaf. **B** Intensity images of characteristic transient levels (I, P, M, T). **C** Amplitude images of major transient characteristics (ID, DP, PS, MT) (Omasa et al. 1987)

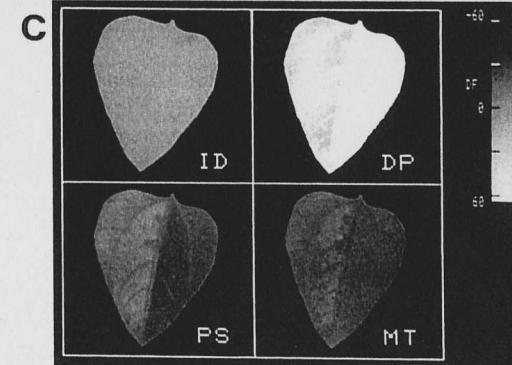
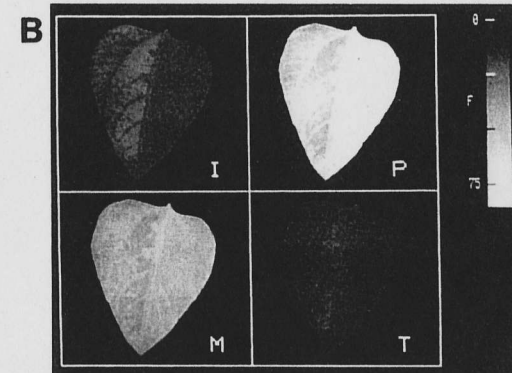
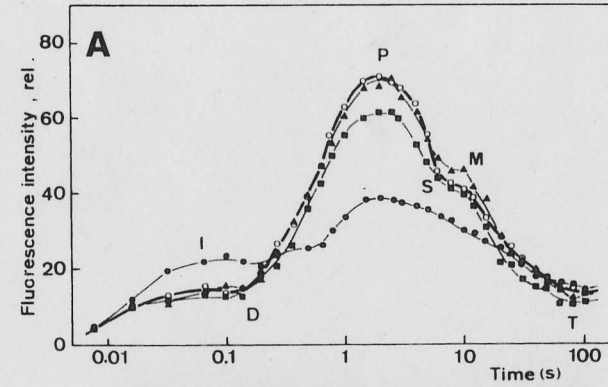


Fig. 19A-C. Recovery of CFI from disturbances by SO_2 . After the measurement described in Fig. 18, the same plant was kept at 25.0°C air temperature and 70% RH in darkness and SO_2 -free air. Measurement of CFI was then repeated for the same leaf every 60 min. The CFI measured at 6 h after the initiation of SO_2 fumigation are presented. **A** CFI curves at leaf sites marked in Fig. 18A; **B** intensity images of characteristic transient levels; **C** amplitude images of major transient characteristics. Symbols are the same as those in Fig. 18 (Omasa et al. 1987)

In general, the leaf area close to the veinal region was resistant to SO₂-fumigation. The resistance is probably due to the smaller absorption of SO₂ in the proximity of veins, because of the small stomatal conductance in these areas and/or to the fast dilution of absorbed SO₂ by the larger provision of water from the vein (Omasa et al. 1981b; 1985a). Therefore, we observed that SO₂ injured the leaf heterogeneously, and the recovery from the SO₂ injury also proceeded heterogeneously. Although the heterogeneous response of a plant leaf to environmental stress is a common process microscopically, the conventional method (Schreiber et al. 1975; Schreiber 1983), which measures the 'averaged' CFI derived from a defined leaf area, could not resolve a spatially different response in the same leaf. For example, Shimazaki et al. (1984) described the partial recovery of O₂ evolution and CFI from the SO₂ injury in a spinach leaf macroscopically. Such a partial recovery is probably due to the combination ('average') of the complete and incomplete recovery, as indicated in the present investigation.

As shown above, our image instrumentation system demonstrated not only the affected location in photosynthetic activity on the leaf but also the inhibition site in the photosynthetic electron transport system. The phytoluminographic technique, which measures the DLE spatially over the single whole leaf, was developed to detect injury to the photosynthetic activity (Björn and Forsberg 1979; Ellenson and Amundson 1982). This method detects the injured area on the leaf in photosynthetic activity but does not reveal the inhibition site in the photosynthetic system, because the intensity of the DLE is very similarly reduced by various factors; these include inhibition of the oxidizing and reducing sides of PSII, uncoupling of photophosphorylation, anaerobic conditions, and high CO₂ conditions (Sato and Katoh 1983). On the contrary, the CFI imaging points to SO₂ fumigation, inhibiting the oxidizing side of PSII.

Together with the techniques of computerized image processing, such as DLE imaging and thermal imaging, which provide information about stomatal response and gas exchange, the image analysis of CFI provides an integrative approach for early warning diagnosis and for functional analysis of disorders during stress, as well as for the plant's capacity to recover.

6 Thermal Image Instrumentation

The rate of physiological reactions in living plants is dependent upon cell temperature (Sutcliffe 1977, Berry and Björkman 1980, Sakai and Larcher 1987), which, in turn, is determined by the conditions of the thermal environment (i.e., air temperature, humidity, radiation, and air currents) (Monteith 1973, Jones 1983). As such, when plants are kept under a uniform thermal environment, leaf temperature can indirectly provide physiological information on stomatal movement, transpiration, CO₂ uptake, and air pollution absorption (Hashimoto et al. 1984, Omasa and Aiga 1987). Thermal image instrumentation is a method for obtaining plant temperatures and the physiological information involved in it, by measuring the electromagnetic waves of the thermal

infrared band (Omasa et al. 1980, 1981a,b,c; Horler et al. 1980; Hashimoto et al. 1984).

6.1 Method for Measuring Plant Temperature and Its Accuracy

Thermal infrared radiation from the environment (approximately 10 μm) is almost all absorbed by the plant. However, since thermal infrared radiation is emitted from the plant according to Planck's law of radiation, the plant temperature can be obtained by measuring the radiation in this band.

For a perfectly diffuse and opaque plant surface the spectral energy of infrared radiation from the surface at temperature T is R(λ, T, T_s), given by:

$$R(\lambda, T, T_s) = \epsilon(\lambda, T)W(\lambda, T) + [(1 - \epsilon(\lambda, T))E(\lambda, T_s)], \quad (1)$$

where λ is the wavelength, ε(λ, T) is the spectral emissivity of the plant surface, W(λ, T) is the spectral radiant energy of a black body at temperature T, and E(λ, T_s) is the spectral radiant energy from the environment at temperature T_s to the plant surface.

When R(λ, T, T_s) is measured by an infrared detector with spectral sensitivity in the band from λ₁ to λ₂, the output voltage V_T(T, T_s) of the detector is:

$$V_T(T, T_s) = \int_{\lambda_1}^{\lambda_2} f(\lambda)R(\lambda, T, T_s)d\lambda \\ \approx \bar{\epsilon}(T)V_w(T) + [1 - \bar{\epsilon}(T)]V_E(T_s), \quad (2)$$

where

$$\bar{\epsilon}(T) = \frac{[\int_{\lambda_1}^{\lambda_2} \epsilon(\lambda, T)f(\lambda)W(\lambda, T)d\lambda]}{[\int_{\lambda_1}^{\lambda_2} f(\lambda)W(\lambda, T)d\lambda]}, \\ V_w(T) = \int_{\lambda_1}^{\lambda_2} f(\lambda)W(\lambda, T)d\lambda,$$

and

$$V_E(T_s) = \int_{\lambda_1}^{\lambda_2} f(\lambda)E(\lambda, T_s)d\lambda,$$

since f(λ) is the function describing the radiation-electricity conversion of the detector, the amplification with the amplifier, and the transmission and reflection of the air, lens, filter, etc.; $\bar{\epsilon}(T)$ is the average emissivity in the band from λ₁ to λ₂; V_w(T) is the output voltage in the measurement of W(λ, T), and V_E(T_s) is the output voltage in the measurement of E(λ, T_s).

When $\bar{\epsilon}(T)$ and V_E(T_s) are given, V_w(T) can be obtained from V_T(T, T_s):

$$V_w(T) = [V_T(T, T_s) - V_E(T_s)] / \bar{\epsilon}(T) + V_E(T_s). \quad (3)$$

Furthermore, the plant temperature T is evaluated from V_w(T) using the characteristic relation between T and V_w(T).

The emissivity $\bar{\epsilon}(T)$ of the plant in the spectral sensitivity range (8–13 μm) of the thermal camera is 0.95 to 0.99 (Fuchs and Tanner 1966; Omasa et al. 1980). The influence of radiation from the environment is corrected by adjusting V_E(T_s) in Eq. (3). The influence of the change in f(λ) is also corrected by continuously monitoring a standard blackbody source within the camera. As a result, it is possible to measure the plant temperature with an accuracy of ± 0.1 °C (Omasa et al. 1980).

A thermal camera of the optical-mechanical scanning type, called a thermography, with a InSb (3.5–5.5 μm) or HgCdTe (8–13 μm) detector, is now on the market. To use for plant measurements, the scanning type of mirror vibration, which has good temperature sensitivity and resolution, is better than that of prism rotation. Since the detector is cooled by liquid nitrogen (77K), it is necessary to supplement it every few hours. At present, the detector with an electronic cooler (200K) and the new image sensor of the electrical scanning type cannot be used to accurately measure plant temperature because of insufficient sensitivity and resolution.

Figure 20 shows our thermal image instrumentation system and blackbody source for calibration. The thermal camera (JEOL JTG-IBL) is an optical-mechanical scanning type, and its detector is an HgCdTe (8–13 μm , cooled by liquid nitrogen). The detected signals from the thermal camera are converted into 12-bit digital signals (256H \times 240V, quantization error 0.0125 $^{\circ}\text{C}$) by a thermal image processor and analyzed by a host computer. The detected image is enhanced by integrating, using the thermal image processor. The temperature resolving power, the uniformity of image, and the drift is within 0.05 $^{\circ}\text{C}$, $\pm 0.1^{\circ}\text{C}$ and $\pm 0.05^{\circ}\text{C}/4\text{ h}$ respectively. The image resolution is ca. 50H \times 40V in measuring at 4% error (0.2 $^{\circ}\text{C}$) (Omasa et al. 1981a). Emissivity of the blackbody source (Electro Optical Industries PD1401X) is 0.99, and the surface temperature is automatically controlled at 0.05 $^{\circ}\text{C}$ accuracy.

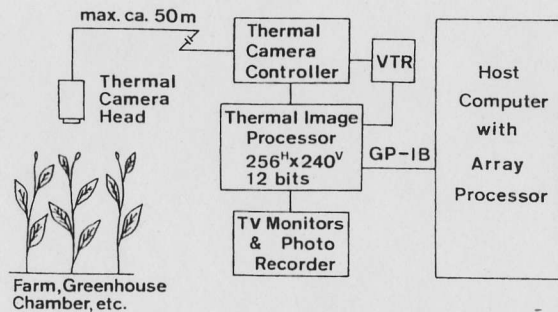


Fig. 20. Thermal image instrumentation system and blackbody source for calibration

6.2 Evaluation of Stomatal Response, Transpiration, and Gas Sorption

Plants and the surrounding atmosphere exchange CO_2 and water vapor, which are related to photosynthesis, respiration, and transpiration, through the stomata. In atmospherically polluted areas, toxic air pollutants also enter the plants through the stomata, and have various effects.

By analyzing relationships between leaf temperature and thermal environment factors such as air temperature, humidity, radiation, and air currents, from the standpoint of the plant-environment system, the spatial distributions of the transpiration rate, stomatal resistance to water vapor-diffusion (which is an indicator of stomatal aperture), and gas absorption are exactly evaluated from the leaf temperature (Omasa et al. 1981a,b,c). In the case of evaluating them at local sites over a thin flat leaf, the model is simplified as follows:

The transpiration rate W_x ($\text{gcm}^{-2}\text{s}^{-1}$) at local site x on the leaf is:

$$W_x = [\alpha_p E_{sx} + \epsilon \{E_{wx} - 2\sigma (273.15 + T_{lx})^4\} + 2\rho C_p (T_a - T_{lx}) / r_{kax}] / L, \quad (4)$$

where E_s is shortwave radiation from the environment (wavelength $< 3\mu\text{m}$, $\text{calcm}^{-2}\text{s}^{-1}$), E_w is longwave radiation from the environment (wavelength $> 3\mu\text{m}$, $\text{calcm}^{-2}\text{s}^{-1}$), α_p is absorption coefficient of shortwave radiation of the leaf, ϵ is emissivity of longwave radiation of the leaf, T_l is leaf temperature ($^{\circ}\text{C}$); T_a is air temperature ($^{\circ}\text{C}$), σ is Stefan-Boltzmann constant ($\text{calcm}^{-2}\text{s}^{-1}\text{K}^{-4}$), ρC_p is volumetric heat capacity of air ($\text{calcm}^{-3}\text{C}^{-1}$), r_{kax} is boundary layer resistance to heat transfer, and L is latent heat by evaporation (calg^{-1}). The subscript x denotes the values at local site x on the leaf. Assuming that thermal environment factors such as air temperature, humidity, radiation, and air current are kept constant all over the leaf, the only variable in the right side of Eq. (4) is leaf temperature T_{lx} . Therefore, by previously determining the parameters other than T_{lx} , the transpiration rate W_x is evaluated from T_{lx} , measured with the thermal instrumentation system. The stomatal resistance to water vapor diffusion, r_{wax} (scm^{-1}), is furthermore expressed by:

$$r_{wax} = 2 \{X_{sx}(T_{lx}) - \phi X_s(T_a)\} / W_x - (\kappa / D_w)^{2/3} r_{kax}, \quad (5)$$

where $X_s(T)$ is saturated water vapor density at T $^{\circ}\text{C}$, ϕ is relative humidity, κ is thermal diffusivity of air, and D_w is air-water vapor diffusivity. The absorption rate Q_x ($\text{gcm}^{-2}\text{s}^{-1}$) of CO_2 or air pollutants at a local site x is evaluated by the following equation:

$$Q_x = 2(P_a - P_{lx}) / (r_{gax} + r_{gsx}), \quad (6)$$

where

$$r_{gax} = (\kappa / D_g)^{2/3} r_{kax}$$

$$r_{gsx} = (D_w / D_g) r_{wsx},$$

since P_a is atmospheric gas concentration (gcm^{-3}); P_l is gas concentration at the gas-liquid interface in the substomatal cavity (gcm^{-3}), r_{ga} is boundary layer resistance to gas diffusion (scm^{-1}), r_{gs} is stomatal resistance to gas diffusion (scm^{-1}), and

D_g is air-gas diffusivity (cm^2s^{-1}). The gas concentration P_{1x} of SO_2 , NO_2 , O_3 and PAN (major air pollutants) at the gas-liquid interface in the sub-stomatal cavity has been assumed to be zero $\mu\text{mol l}^{-1}$, because physiological functions such as metabolism and transfer which reduce the gas concentration, are considered sufficient (Omasa 1979; Omasa et al. 1979). However, the CO_2 concentration concerned with photosynthesis and respiration is changed by conditions of environment and growth (Omasa 1979; Jones 1983).

Figure 21 shows changes in the spatial distributions of stomatal resistance to water vapor diffusion, transpiration rate, and O_3 absorption rate evaluated from leaf temperature images of a sunflower plant during exposure to $1.2 \mu\text{mol l}^{-1}$. During the O_3 exposure, the stomatal resistance increased, and the transpiration rate decreased, because of stomatal closure. However, their behaviors varied randomly at different sites on the leaf. This result means that stomatal sensitivity to O_3 varies at the local site of the leaf. By this method, the transpiration rate, stomatal resistance, and gas absorption rate are evaluated with errors of $0.02 \times 10^{-6} \text{gcm}^{-2}\text{s}^{-1}$, 0.3scm^{-1} , and ca. 10% respectively. (Omasa et al. 1981a,b,c).

It is very difficult to evaluate exactly the stomatal resistance and transpiration rate of plants growing in the field. However, since stomatal closure occurs before the appearance of visible leaf injury, thermal image instrumentation can be used for the early detection of plant stress under steady-state thermal environments. Figure 22 demonstrates the diagnosis of some zelkova trees on Aoba street in Sendai city. A tree on the left was high in leaf temperature because of stomatal closure caused by gasoline and water stress, although damage was not visible. The use of both thermal image instrumentation and portable porometer (e.g., LI-COR, Model LI-1600) makes a precise diagnosis of field plants possible.

The leaf temperature image is also used for screening plants. In Fig. 23, the leaf temperature of a poplar tree was lower than that of a white oak and a spindle tree. This indicates that the poplar tree has large transpiration and gas absorption rates, and potential for growth and air purification.

7 Computed Tomography

Computed tomography (CT), first developed in the medical field and currently undergoing remarkable further development, is an effective method for investigating conditions in a living organism without destroying it (Herman 1979; Onoe 1982; Mansfield and Morris 1982). Cormack and Hounsfield were awarded the Nobel Prize in Physiology and Medicine in 1979 for developing the X-ray CT (Hounsfield 1973) which is now popularly used in clinical medicine and in industry. In addition to X-ray CT, CTs using radioisotopes (RI), including positron CT, and CTs using an energy medium such as ultrasonic waves, nuclear magnetic resonance (NMR or MR), heavy particle beams or microwaves are currently being studied, partly for practical use. Methods for investigating objects at the cell level are now being developed. In the plant field, investigations of annual rings and internal rot in living trees by X-ray CT, and studies of root systems and water absorption of

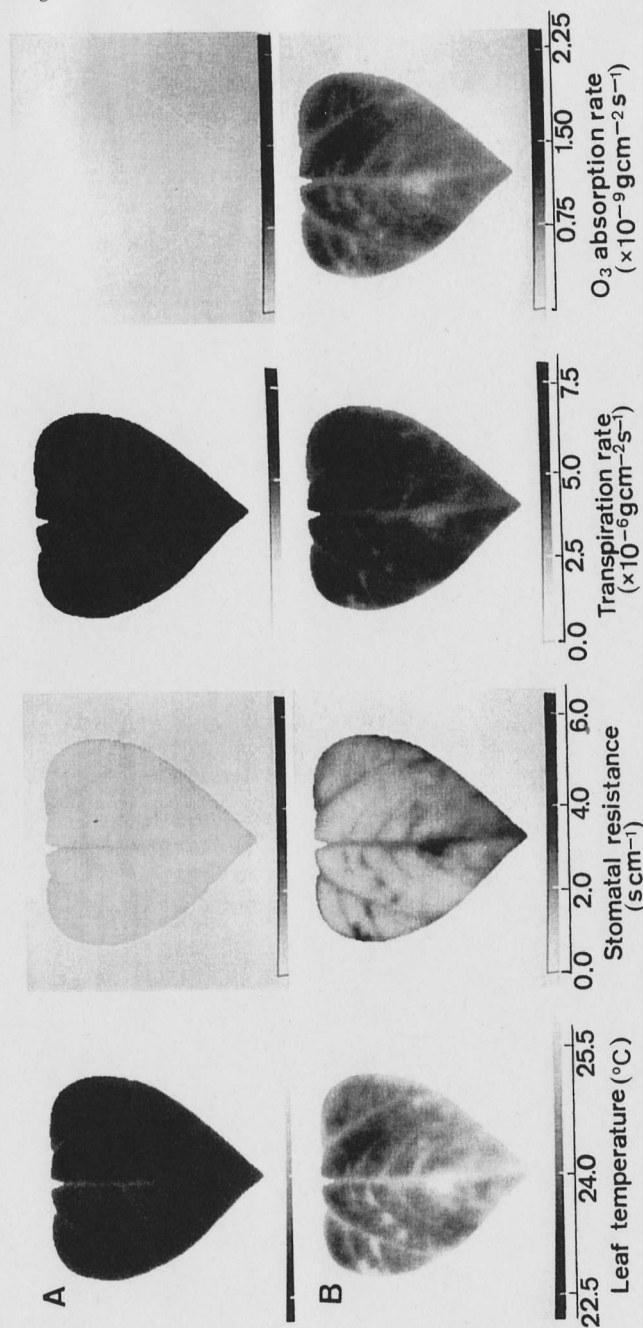


Fig. 21A-B. Changes in spatial distributions of stomatal resistance to water vapor diffusion, transpiration rate, and O_3 absorption rate evaluated from leaf temperature images of a sunflower plant during exposure to $1.2 \mu\text{mol l}^{-1}$. A Just before exposure; B 30 min after exposure start. The distributions of shortwave radiation, longwave radiation, illumination, and boundary layer resistance to heat transfer on the leaf surface were maintained at $2.37 \pm 0.05 \times 10^{-3} \text{cal cm}^{-2}\text{s}^{-1}$, $2.23 \pm 0.01 \times 10^{-2} \text{cal cm}^{-2}\text{s}^{-1}$, ca. 25 klx, and $1.5 \pm 0.1 \text{s cm}^{-1}$, except at the leaf edges. Other environmental conditions: air temperature, $25.0 \pm 0.1^\circ\text{C}$; RH, $62 \pm 1\%$ (After Omasa et al. 1981c)

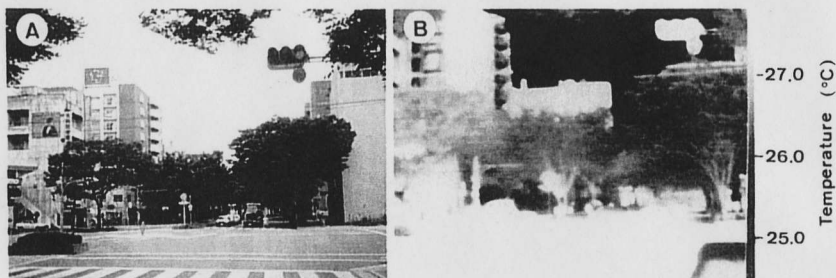


Fig. 22A,B. Diagnosis of zelkova trees on Aoba street in the city of Sendai. A Photograph; B thermal image. Environmental conditions: air temperature 26.5°C; light intensity, about 500 μmol photons m⁻²s⁻¹ (Omasa et al. 1990)

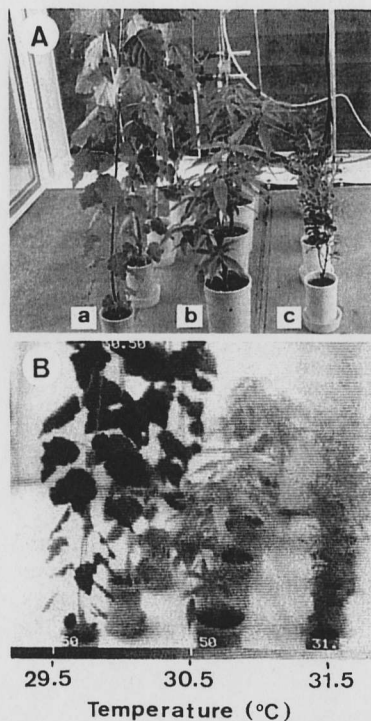


Fig. 23A,B. Difference in leaf temperature of various healthy plants. A Photograph (a poplar tree; b white oak tree; c spindle tree); B thermal image. Environmental conditions: air temperature, 31.0°C; RH, 70%; light intensity, 500 μmol photons m⁻²s⁻¹ (unpublished data)

plants by MRI (magnetic resonance imaging), are now being studied, and their future development is expected to continue.

7.1 Instrumentation of Living Trees by X-Ray CT

X-ray CTs, widely used in clinical medicine and industry, are suitable for obtaining information about the internal structure of a living organism. Portable equipment, suitable for field instrumentation, has been developed recently, and is powerful enough for investigation and diagnoses of annular rings and internal rot in living trees (Onoe et al. 1983). Although various methods for obtaining a reconstructed image from X-ray projection images have been proposed, an easily understood method based on Fourier's projection theorem is shown in Fig. 24.

Projection $p(s, \theta)$ of a subject with a density distribution of $f(x, y)$ to the s axis, with rotation angle θ to the x axis is given by the following equation, by assuming a t axis perpendicular to the s axis:

$$p(s, \theta) = \int_{-\infty}^{\infty} f(x, y) dt \tag{7}$$

The two-dimensional Fourier transformation $F(u, v)$ of $f(x, y)$ is given by:

$$F(u, v) = \iint_{-\infty}^{\infty} f(x, y) \exp[-j2\pi(ux + vy)] dx dy \tag{8}$$

Recognizing that $s = x \cos\theta + y \sin\theta$ and $t = -x \sin\theta + y \cos\theta$, the one-dimensional Fourier transformation $P(w, \theta)$ of $p(s, \theta)$ relating to the s is obtained and rearranged:

$$\begin{aligned} P(w, \theta) &= \int_{-\infty}^{\infty} p(s, \theta) \exp(-j2\pi ws) ds \\ &= \iint_{-\infty}^{\infty} f(x, y) \exp[-j2\pi w(x \cos\theta + y \sin\theta)] dx dy \\ &= F(w \cos\theta, w \sin\theta) \end{aligned} \tag{9}$$

This relationship, called projection theorem, means that the one-dimensional Fourier transformation of projection is equal to a center-cross-section gained by cutting the two-dimensional Fourier transformation of the original distribution to the angle. Therefore, projections from various directions allow the production of

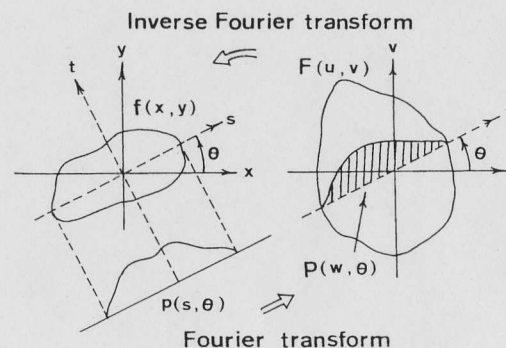


Fig. 24. The concept of Fourier's projection theorem

$F(u,v)$, and an inverse Fourier transformation of $F(u,v)$ reconstructs the original image:

$$f(x,y) = \iint_{-\infty}^{\infty} F(u,v) \exp [j2\pi (ux + vy)] \, du \, dv \quad (10)$$

Changes of variables, $u = w \cos \theta$ and $v = w \sin \theta$, are performed and the integral limit relating to θ is halved to obtain Eq. (11):

$$f(x,y) = \int_{-\infty}^{\infty} |w| \, dw \int_0^{\pi} d\theta P(w,\theta) \exp (j2\pi ws). \quad (11)$$

If the integral order is changed, the integral relating to w is the inverse Fourier transformation of $|w| P(w,\theta)$. This is set as $q(s,\theta)$, and Eq. (12) is obtained:

$$q(s,\theta) = \int_{-\infty}^{\infty} |w| P(w,\theta) \exp (j2\pi ws) \, dw. \quad (12)$$

As a result, Eq. (11) becomes the following:

$$f(x,y) = \int_0^{\pi} q(s,\theta) \, d\theta. \quad (13)$$

In Eq. (12), q is an inverse transformation of the product of $|w|$ and P . The product of the Fourier transformation in the frequency domain is a convolution in the space domain. Therefore, q is calculated by convoluting the inverse transformation of filter $|w|$ to eliminate blur in the original projection p . Actual processing differs depending on the equipment, and various methods have been proposed.

Portable X-ray CT equipment developed by Onoe et al. (1983) is shown in Fig. 25. In the equipment, an X-ray tube of 40–120 kV and three NaI scintillation counters are used. The tube and the detectors are relatively fixed in an assembly, which rotates around the target focus of the X-ray tube, so that three collimated X-ray beams, 8° apart, scan across the object under test. The target focus is eccentric from the center of the tree, hence a fan-beam algorithm is used for reconstruction. Typically, 1200 samples of 16 bits of projection data are taken in 2° intervals.

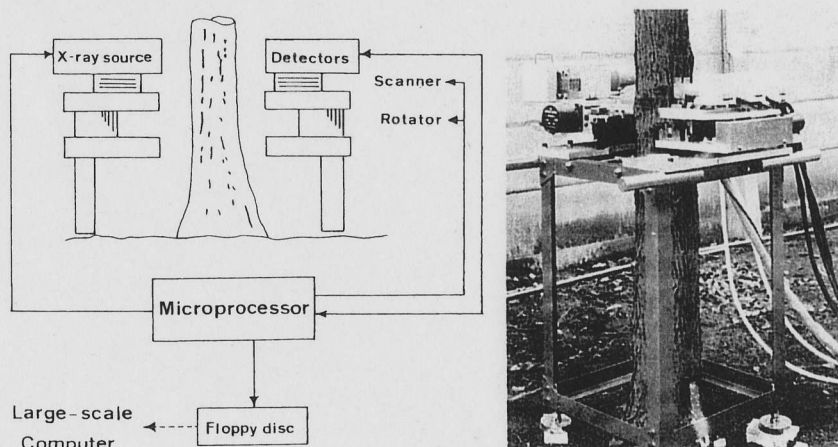


Fig. 25. Portable X-ray CT measuring a living tree (After Onoe et al. 1983)

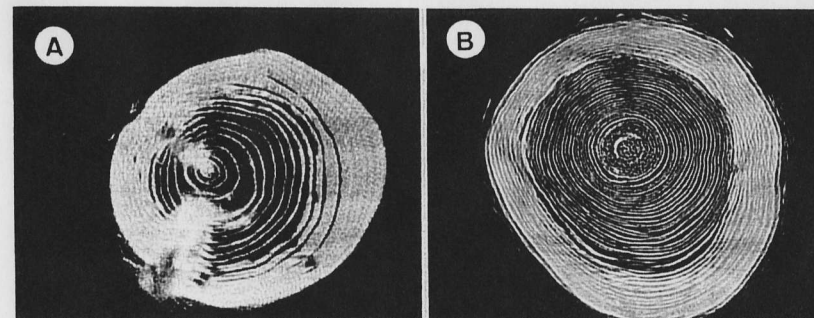


Fig. 26A,B. Reconstructed images of living Japanese cedar and hinoki trees. A Japanese cedar tree; B hinoki tree. Large X-ray absorption parts are white and small parts are black. The annual rings in B are enhanced by unsharp masking (Onoe et al. 1983)

Scanning, rotation, and data collection are controlled by a microprocessor. The projection data is stored in a floppy disc, and calculations for the reconstruction are carried out by a large-scale computer.

Figure 26 shows reconstructed images of living Japanese cedar and hinoki trees. Large X-ray absorption parts are white and small parts are black, although the annual rings in B are enhanced by unsharp masking. In the reconstructed images, annual rings, differences in water content, and knots (Japanese cedar) are observed. Since cut and dried woods differ in X-ray absorption, because of a difference in growth density of springwood and summerwood, the annual rings are easily distinguishable. However, it is difficult to observe the annual rings of a standing tree containing water. This tendency is particularly strong in the sapwood, which is a passageway for the transpiration flow, and which has more water content than the heart wood. Therefore, enhancement of the annual rings is required.

The formation of annual rings is greatly affected by changes in the environment. Therefore, environmental changes at each growth stage are estimated by investigating the growth in annual rings of standing trees using the portable X-ray CT. Also, since the CT gives information about rot and water content in addition to that about annual rings, it can be used to investigate the growth conditions of trees needing protection.

7.2 Instrumentation of Root Systems and Soil Moisture by MRI

Nuclear magnetic resonance (NMR or MR) instrumentation methods are widely used in the fields of biological and medical research as an analytical means for obtaining information about the chemical composition and reaction process in organisms, from the resonance phenomena between the magnetic moment of the nuclear spin system and the impressed magnetic field (Linskens and Jackson 1986). Since Lauterbur (1973) announced it in 1973, an MR imaging method

(Zeugmatography) using a linear magnetic field gradient has attracted considerable attention as a diagnostic method for clinical medicine. It is characterized as a useful method for providing not only morphological information about organisms but also physiological and biochemical information, and also for easily providing images of any section, by electrical control of the impressed magnetic field. Superconductive magnet MRIs with a high resolution as good as that obtained by X-ray CT have been developed recently, and success in imaging at cell level has been announced (Aguayo et al. 1986). At present, commercially available MRIs can give information relating to density, T_1 (spin-lattice relaxation time), and T_2 (spin-spin relaxation time), etc., for proton (hydrogen atomic nucleus).

Figure 27 shows the concept of the MRI. The nucleus of the atoms (e.g., hydrogen) which make up organisms has a positive charge and spins like the earth. When the nucleus is placed in a magnetic field, it oscillates like a top (Larmor precession) at a frequency proportional to the field intensity. Here, an impression of a high-frequency magnetic field at the same frequency as that of the precession causes a resonance, and the nucleus absorbs its energy and becomes excited-state. The high-frequency field is then cut, and the nucleus returns to the original state, while releasing the absorbed energy (relaxation phenomenon). The energy released from the nucleus at this time is measured as FID (free induction decay) or SE (spin echo) signals, to make a tomographic image. In concrete terms, a linear gradient magnetic field, in which the change in intensity depends linearly on the position, is produced by the addition of an inclined magnetic field to a static magnetic field. Under this condition, a specific high-frequency magnetic field is impressed, so that just the nuclei located in a certain section are excited (selective irradiative process). After this, the inclined magnetic field is turned off, and a newly inclined magnetic field is put on the excited section to produce a linear gradient magnetic field. In this way, the output signal is obtained as a synthetic signal of frequencies corresponding to the respective magnetic field intensity. The Fourier transformation of this signal

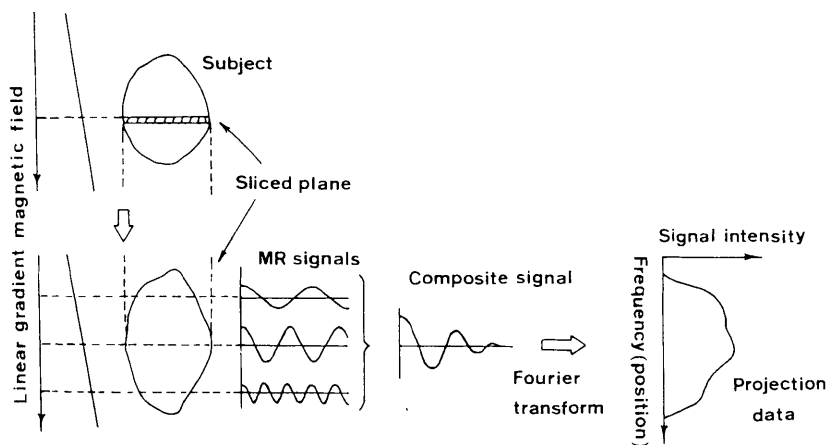


Fig. 27. The concept of MRI

gives the same projection data as that from X-ray CT. The direction of the linear gradient magnetic field on the excited section is changed to obtain projection data in each direction. A reconstructed image is calculated from a series of the projection data by the same method as X-ray CT. Actual processing differs depending on the equipment, and various other imaging methods have been proposed.

Resonance frequencies of high-frequency magnetic fields are in RF (radio-frequency) wave; for protons (^1H), 42.6 MHz at 1 T (Tesla). The magnetic field is impressed by the SR (saturation recovery) method, the IR (inversion recovery) method, and the SE method, etc. The SE method is frequently used because it detects signals easily. In this method, first a 90° pulse is impressed to excite the system and, after τ (echo time) elapses, a 180° pulse is applied. The FID signal after the 90° pulse and the SE signal, which has a peak at τ elapses after the 180° pulse, are then detected. The intensity I_{SE} of the SE image is proportional to the xy component of magnetization at occurrence time of echo and an approximation is given by the following equation:

$$I_{SE} = k\rho_p \exp(-2\tau/T_2) [1 - \exp(-T_r/T_1)], \quad (14)$$

where k , ρ_p , and T_r are constant, proton density, and repetition time of the pulse series respectively. I_{SE} , if τ is sufficiently small, is expressed by:

$$I_{SE} = k\rho_p [1 - \exp(-T_r/T_1)], \quad (15)$$

and agrees with the image (SR image) obtained from the SR method. Here, if T_r is made sufficiently larger than T_1 , the image shows proton density. If τ is made large, $\exp(-T_r/T_2)$ has an effect and the influence of T_2 appears. In addition, it is possible to obtain T_1 and T_2 images with information related to phase or viscosity, but this is not advisable from the points of view of S/N and calculation time.

As an example of MR imaging of plants, distributions of root systems and soil moisture were measured by Omasa et al. (1985b) and Bottomley et al. (1986). Figure 28 shows ^1H images of dry and wet soils with broad bean roots in horizontal sections of pots. The gray level indicated by the numerals under the gray scale shows the intensity of the MR signal. The MR signal from air-dried soil (ca. pF 5.5) in A was very weak except for that from the root in the center, and the background noise was observed as black-and-white spots. The wet soil (ca. pF 2) in B showed high gray level, although the level differed from region to region in the pot. Since the bulk of protons in soil is water, the gray level represents its water content, T_1 and T_2 . Care needs to be taken concerning image distortion caused by diamagnetism and ferromagnetism of soils (Bottomley et al. 1986).

Figure 29 shows an ^1H image of a broad bean and its main root in a vertical section of a pot with wet soil. Since the gray level of the bean and root was higher than that of the soil, we could easily discriminate the bean and its main root from the soil. However, roots finer than 2 mm could not be detected by our CT system. The lack of uniformity in the soil-water content was probably influenced by the water uptake of roots, as well as by the spatial distribution of the soil structure. Recent developments in MRI technology have increased the spatial resolution to 0.05 mm, making it possible to observe differences in the water content of various tissues of plant organs (Fig. 30) (Brown et al. 1986).

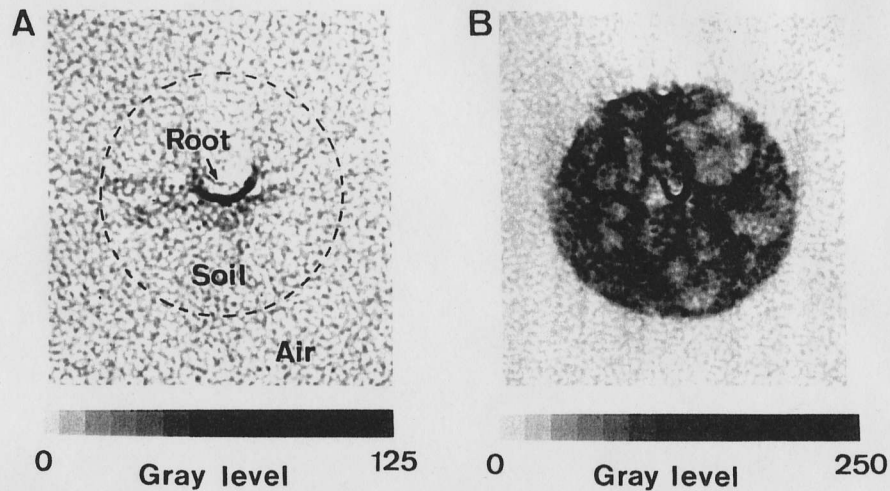


Fig. 28A,B. ^1H images of dry and wet soils with broad bean roots in horizontal sections of pots. A Air-dried soil; B wet soil. The gray level indicated by the numerals under the gray scale shows the intensity of MR signal. Parameters: $T_r = 525$ ms, $\tau = 40$ ms (Omasa et al. 1985b)

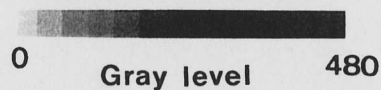


Fig. 29. ^1H image of a broad bean and its main root in a vertical section of a pot with wet soil. Parameters: $T_r = 525$ ms, $\tau = 40$ ms (Omasa et al. 1985b)

The results suggest that the MR imaging is an effective method for measuring spatial distributions of water in soil and roots. By analyzing the image, information about the growth in seedling and root, and the water uptake of the root, may be provided without destroying the plant itself and the soil environment. Since an MR signal, especially T_2 , relates to water potential as well as to water content in plants (Van As 1982), the CT system also may be used to measure spatial distributions of water potential. The MRI is more suitable for making three dimensional images, in comparison with X-ray CT.

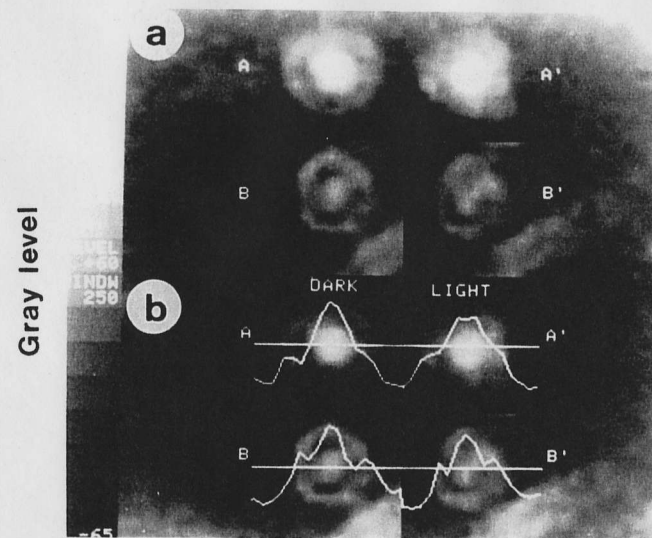


Fig. 30. Microscopic ^1H images of changing water content in *Pelargonium hortorum* roots. a Images of cross-sections of adventitious roots showing apparent changes in distribution of water after a period of transpiration. Roots A and B represent the plant imaged in the dark, and A' and B' represent the roots imaged after the plant was exposed to light and allowed to transpire for 8 h. b Graphs superimposed on the corresponding image represent the relative MR signal intensity for each pixel on its respective transecting line. These graphs better illustrate changes in signal intensity caused by changes in proton concentration within the root during transpiration. Parameters: $T_r = 400$ ms; $\tau = 20$ ms (After Brown et al. 1986)

Another application of MRI has been to detect the presence of postharvest internal disorders in stored fruit. In apples, avocados, and pears, MRI clearly revealed the extent of breakdown in the core tissue. (Omasa et al. 1989, Wang and Wang 1989).

References

- Aguayo JB, Blackband SJ, Schoeninger J, Mattingly MA, Hintermann M (1986) Nuclear magnetic resonance imaging of a single cell. *Nature (Lond)* 322:190-191
- Berry J, Björkman O (1980) Photosynthetic response and adaptation to temperature in higher plants. *Annu Rev Plant Physiol* 31:491-543
- Björn LO, Forsberg AS (1979) Imaging by delayed light emission (photoluminography) as a method for detecting damage to the photosynthetic system. *Physiol Plant* 47:215-222
- Bottomley PA, Rogers HH, Foster TH (1986) NMR imaging shows water distribution and transport in plant root systems in situ. *Proc Natl Acad Sci USA* 83:87-89
- Brown JM, Johnson GA, Kramer PJ (1986) In vivo magnetic resonance microscopy of changing water content in *Pelargonium hortorum* roots. *Plant Physiol* 82:1158-1160
- Colwell RN (ed) (1983) Manual of remote sensing, 2nd edn, vols 1 & 2. Am Soc Photogrammetry, Falls Church
- Ellenson JL (1985) Phytoluminographic detection of dynamic variations in leaf gaseous conductivity. *Plant Physiol* 78:904-908
- Ellenson JL, Amundson RG (1982) Delayed light imaging for the early detection of plant stress. *Science* 215:1104-1106
- Ellenson JL, Raba RM (1983) Gas exchange and phytoluminography of single red kidney bean leaves during periods of induced stomatal oscillations. *Plant Physiol* 72:90-95

- Fuchs M, Tanner CB (1966) Infrared thermometry of vegetation. *Agron J* 58:597-601
- Gates DM, Keegan HJ, Schleter JC, Weidner VR (1965) Spectral properties of plants. *Appl Opt* 4:11-20
- Hashimoto Y, Ino T, Kramer PJ, Naylor AW, Strain BR (1984) Dynamic analysis of water stress of sunflower leaves by means of a thermal image processing system. *Plant Physiol* 76:266-269
- Heath OVS (1959) The water relations of stomatal cells and the mechanisms of stomatal movement. In: Steward FC (ed) *Plant physiology* vol 2. Academic Press, Lond NY, pp 193-250
- Herman GT (ed) (1979) *Image reconstruction from projection*. Springer, Berlin Heidelberg New York
- Horler DNH, Barber J, Barringer AR (1980) Effects of cadmium and copper treatments and water stress on thermal emission from peas (*Pisum sativum* L.): Controlled environment experiments. *Remote Sens Environ* 10:191-199
- Hounsfield GN (1973) Computerized transverse axial scanning (tomography): Part I. Description of system. *Brit J Radiol* 46:1016-1022
- Jones HG (1983) *Plants and microclimate*. Cambridge Univ Press, Cambridge
- Kappen L, Andresen G, Löscher R (1987) In situ observations of stomatal movements. *J Exp Bot* 38:126-141
- Kautsky H, Appel W, Amann H (1960) Die Fluoreszenzkurve und die Photochemie der Pflanze. *Biochem Z* 332:277-292
- Kendrick RE, Kronenberg GHM (eds) (1986) *Photomorphogenesis in plants*. Nijhoff Publ, Dordrecht
- Knipling EB (1970) Physical and physiological basis for the reflectance of visible and near-infrared radiation from vegetation. *Remote Sens Environ* 1:155-159
- Lauterbur PC (1973) Image formation by induced local interactions - examples employing nuclear magnetic resonance. *Nature (Lond)* 242:190-191
- Linskens HF, Jackson JF (eds) (1986) *Modern methods of plant analysis*. New series vol 2. Nuclear magnetic resonance. Springer, Berlin Heidelberg New York Tokyo
- Mansfield P, Morris PG (1982) NMR imaging in biomedicine. Academic Press, Lond NY
- Matsui T, Eguchi H (1978) Image processing of plants for evaluation of growth in relation to environment control. *Acta Hort* 87:283-290
- Meidner H (1981) Measurements of stomatal aperture and responses to stimuli. In: Jarvis PG, Mansfield TA (eds) *Stomatal physiology*. Cambridge Univ Press, Cambridge, pp 25-49
- Meidner H, Mansfield TA (1968) *Physiology of stomata*. McGraw-Hill, Lond
- Monteith JL (1973) *Principles of environmental physics*. Arnold, Lond
- Monzi M (1939) Die Mitwirkung der Stomata-Nebenzellen auf die Spaltöffnungsbewegung. *Jpn J Bot* 9:373-394
- Murata N, Nishimura M, Takamiya A (1966) Fluorescence of chlorophyll in photosynthetic systems II. Induction of fluorescence in isolated spinach chloroplasts. *Biochim Biophys Acta* 120:23-33
- Myers VI (ed) (1983) Remote sensing applications in agriculture. In: Colwell RN (ed) *Manual of remote sensing*, 2nd ed, vol 2. Am Soc Photogrammetry, Falls Church, pp 2111-2228
- Omasa K (1979) Sorption of air pollutants by plant communities - Analysis and modelling of phenomena. *Res Rep Natl Inst Environ Stud JPN* 10:367-385 (in Japanese)
- Omasa K, Onoe M (1984) Measurement of stomatal aperture by digital image processing. *Plant Cell Physiol* 25:1379-1388
- Omasa K, Aiga I (1987) Environmental measurement: Image instrumentation for evaluating pollution effects on plants. In: Singh MG (ed) *Systems and control encyclopedia*. Pergamon Press, Oxford, pp 1516-1522
- Omasa K, Maruyama S (1990) Study on changes in stomata and their surrounding cells using a nondestructive light microscope system: Responses to changes in water absorption through roots. *J. Agr. Meteorol.* 45:265-270 (in Japanese and English summary)
- Omasa K, Abo F, Natori T, Totsuka T (1979) Studies of air pollutant sorption by plants. (II) Sorption under fumigation with NO₂, O₃ or NO₂ + O₃. *J Agric Meteorol* 35:77-83 (in Japanese and English summary); *Res Rep Natl Inst Environ Stud JPN* 11:213-224 (1980) (in English translation)
- Omasa K, Abo F, Hashimoto Y, Aiga I (1980) Measurement of the thermal pattern of plant leaves under fumigation with air pollutant. *Res Rep Natl Inst Environ Stud Jpn* 11:239-247
- Omasa K, Abo F, Aiga I, Hashimoto Y (1981a) Image instrumentation of plants exposed to air pollutants - quantification of physiological information included in thermal infrared images. *Trans Soc Instrum Control Eng* 17:657-663 (in Japanese and English summary); *Res Rep Natl Inst Environ Stud Jpn* 66:69-79 (1984) (in English translation)
- Omasa K, Hashimoto Y, Aiga I (1981b) A quantitative analysis of the relationships between SO₂ or NO₂

- sorption and their acute effects on plant leaves using image instrumentation. *Environ Control Biol* 19:59-67
- Omasa K, Hashimoto Y, Aiga I (1981c) A quantitative analysis of the relationships between O₃ sorption and its acute effects on plant leaves using image instrumentation. *Environ Control Biol* 19:85-92
- Omasa K, Matsumoto S, Aiga I (1982) Trial manufacture of a portable spectroradiometer. *Proc ann meeting (Sendai)*, *Environ Control Biol* 16-17 (in Japanese)
- Omasa K, Aiga I, Hashimoto Y (1983a) Image instrumentation for evaluating the effects of air pollutants on plants. In: Striker G, Havrilla K, Solt J, Kemeny T (eds) *Technological and methodological advances in measurement* vol 3. North Holland Publ Co, Amst, pp 303-312
- Omasa K, Hashimoto Y, Aiga I (1983b) Observation of stomatal movements of intact plants by using an image instrumentation system with a light microscope. *Plant Cell Physiol* 24:281-288
- Omasa K, Hashimoto Y, Aiga I (1984) Image instrumentation of plants exposed to air pollutants (4) Methods for automatic evaluation of the degree of necrotic and chlorotic visible injury. *Res Rep Natl Inst Environ Stud* 66:99-105
- Omasa K, Hashimoto Y, Kramer PJ, Strain BR, Aiga I, Kondo J (1985a) Direct observation of reversible and irreversible stomatal responses of attached sunflower leaves to SO₂. *Plant Physiol* 79:153-158
- Omasa K, Onoe M, Yamada H (1985b) NMR imaging for measuring root system and soil water content. *Environ Control Biol* 23:99-102
- Omasa K, Shimazaki K, Aiga I, Larcher W, Onoe M (1987) Image analysis of chlorophyll fluorescence transients for diagnosing the photosynthetic system of attached leaves. *Plant Physiol* 84:748-752
- Omasa K, Kondo N, Inoue Y (eds) (1988) *Instrumentation and diagnosis of plants*. Asakura, Tokyo (in Japanese)
- Omasa K, Unno K, Yamada H, Nagano T, Funada S (1989) Diagnosis of fruits and rootcrops by MRI. *Proc joint ann meeting (Tsukuba)*, *Environ Control Biol and Agr Meteorol JPN* 262:263 (in Japanese)
- Omasa K, Tajima A, Miyasaka K (1990) Diagnosis of street trees by thermography: Zelkova trees in Sendai city. *J Agr Meteorol* 45:271-275 (in Japanese and English summary)
- Onoe M (ed) (1982) *Medical image processing*. Asakura, Tokyo (in Japanese)
- Onoe M, Tsao JW, Yamada H, Nakamura H, Kogure J, Kawamura H, Yoshimatsu M (1983) Computed tomography for measuring annual rings of a live tree. *Proc IEEE* 71:907-908; *Nuclear Inst Methods Phys Res* 221:213-220
- Papageorgiou G (1975) Chlorophyll fluorescence: An intrinsic probe of photosynthesis. In: Govindjee (ed) *Bioenergetics of photosynthesis*. Academic Press, Lond N Y, pp 319-371
- Sakai A, Larcher W (1987) Frost survival of plants. Springer, Berlin Heidelberg New York Tokyo
- Satoh K, Katoh S (1983) Induction kinetics of millisecond-delayed luminescence intact *Bryopsis* chloroplasts. *Plant Cell Physiol* 24:953-962
- Schreiber U (1983) Chlorophyll fluorescence yield changes as a tool in plant physiology. I. The measuring system. *Photosynth Res* 4:361-373
- Schreiber U, Groberman L, Vidaver W (1975) Portable, solid-state fluorometer for the measurement of chlorophyll fluorescence induction in plants. *Rev Sci Instrum* 46:538-542
- Sharkey TD, Ogawa T (1987) Stomatal responses to light. In: Zeiger E, Farquhar GD, Cowan IR (eds) *Stomatal function*. Stanford Univ Press, Stanford, pp 195-227
- Shimazaki K, Ito K, Kondo N, Sugahara K (1984) Reversible inhibition of the photosynthetic water-splitting enzyme system by SO₂-fumigation assayed by chlorophyll fluorescence and EPR signal in vivo. *Plant Cell Physiol* 25:795-803
- Shiraishi M, Hashimoto Y, Kuraishi S (1978) Cyclic variations of stomatal aperture observed under the scanning electron microscope. *Plant Cell Physiol* 19:637-645
- Sivak MN, Walker DA (1985) Chlorophyll *a* fluorescence: can it shed light on fundamental questions in photosynthetic carbon dioxide fixation? *Plant Cell Environ* 8:439-448
- Smillie RM, Hetherington SE (1983) Stress tolerance and stress-induced injury in crop plants measured by chlorophyll fluorescence in vivo. *Plant Physiol* 72:1043-1050
- Stålfelt MG (1959) The effect of carbon dioxide on hydroactive closure of the stomatal cells. *Physiol Plant* 12:691-705
- Sutcliffe J (1977) *Plants and temperature*. Edward Arnold, London
- Trebst A, Avron M (eds) (1977) *Encyclopedia of plant physiology*. New series vol 5, Photosynthesis 1. Springer, Berlin Heidelberg New York
- Van As H (1982) NMR, water and plants. PhD thesis, Agricult Univ, Wageningen
- Wang CY, Wang PC (1989) Nondestructive detection of core breakdown in 'Bartlett' pears with nuclear magnetic resonance imaging. *HortSci* 24:106-109